Journal of Electromagnetic Waves and Applications, Vol. 1, No. 1, 19–51, 1992

Polarimetric Signatures of a Canopy of Dielectric Cylinders Based on First and Second Order Vector Radiative Transfer Theory

L. Tsang and C. H. Chan

Electromagnetics and Remote Sensing Laboratory
Department of Electrical Engineering
University of Washington
Seattle, WA 98195, USA

J. A. Kong

Department of Electrical Engineering and Computer Science
Massachusetts Institute of Technology
Cambridge, MA 02139, USA

J. Joseph

General Electric Corporate Research and Development
Schenectady, NY 12301, USA

Abstract—Complete polarimetric signatures of a canopy of dielectric cylinders overlyi
a homogeneous half space are studied with the first and second order solutions of t
vector radiative transfer theory. The vector radiative transfer equations contain a gener
nondiagonal extinction matrix and a phase matrix. The energy conservation issue
addressed by calculating the elements of the extinction matrix and the elements of t
phase matrix in a manner that is consistent with energy conservation. Two methods a
used. In the first method, the surface fields and the internal fields of the dielectric cylind
are calculated by using the fields of an infinite cylinder. The phase matrix is calculate
and the extinction matrix is calculated by summing the absorption and scattering
ensure energy conservation. In the second method, the method of moments is used
calculate the elements of the extinction and phase matrices. The Mueller matrix bas
on the first order and second order multiple scattering solutions of the vector radiati
transfer equation are calculated. Results from the two methods are compared. The vect
radiative transfer equations, combined with the solution based on method of moment
obey both energy conservation and reciprocity. The polarimetric signatures, copolariz
and depolarized return, degree of polarization, and phase differences are studied as
function of the orientation, sizes, and dielectric properties of the cylinders. It is show
that second order scattering is generally important for vegetation canopy at C band a
can be important at L band for some cases.

I. INTRODUCTION

Recently, there has been growing interest in polarimetric microwave remote sen
ing of geophysical terrain [1–5]. Some of the prominent features in terrain si
natures [6–8] are a pedestal in copolarized return and in depolarized return, e

hibition of partial polarization with a degree of polarization less than unity on averaging the return signals, and a polarization phase difference between vv and hh waves. The theoretical models of volume scattering that have been studied include the random medium model [9], Rayleigh spherical scatterers [10], simple scattering models [6], small spheroidal scatterers [11], dense medium model [11,12], finite cylinder and discs scattering models [13], and multiple scattering solution [11,14].

Theoretically, the polarimetric signatures of geophysical terrain can be represented by the Mueller matrix. A very common method of calculating the Mueller matrix is through the vector radiative transfer equation [2] governing the propagation and scattering of the four Stokes parameters in a medium containing a random distribution of scatterers. Solutions of the vector radiative transfer theory include the first order solution, the second order solution [11,15], and the full multiple scattering solution for small spherical and non-spherical scatterers [11,14]. It has been shown that the vector radiative transfer equation obeys energy conservation if the scattering amplitude functions used are that of the exact solution of Maxwell's equations for that particular type of scatterers (e.g. Mie scattering by spheres) [2,11]. For the case when approximate expressions are used for the scattering amplitudes, it has been pointed out that care must be exercised in calculating the elements of the extinction matrix and the elements of the phase matrix in a manner that is consistent with energy conservation [11]. The problem of energy conservation is particularly important for multiple scattering problems when violation of energy conservation can lead to nonphysical results. (Note: imagine what will happen if albedo is larger than unity). For the case of scattering by finite cylinders, a common model of approximation was based on the surface field or the internal field of an infinite cylinder to calculate the extinction matrix and the phase matrix. In those cases, however the issue of energy conservation for scattering by a cylinder of finite length has not been addressed [13,16–18]. Conservation of energy in scattering by a single particle is the classical subject of the forward scattering theorem [19,20]. In a medium consisting of a random distribution of many particles with a certain orientation distribution, the situation is different as characteristic waves exist with characteristic polarizations as dictated by Foldy's approximation and the extinction matrix of transfer theory [2,11]. Extinction is described by extinction rates of these characteristic waves. The energy conservation of the extinction matrix, emission vector, and phase matrix of the vector radiative transfer theory is shown to be obeyed if exact scattering amplitudes of the particle is used [2,11]. Reciprocity is also obeyed in vector radiative transfer theory if the exact scattering amplitudes are used [2,11]. On the other hand, the use of the infinite cylinder approximation [16–18] does not give reciprocal bistatic scattering amplitudes. Single scattering by a forest canopy overlying the ground makes use of bistatic scattering amplitudes of the particle in addition to monostatic scattering amplitudes as the wave can be scattered by the particle and then reflected by the ground before reaching the receiver. Thus using the infinite cylinder approximation in scattering by a vegetation canopy overlying the ground can give different results for HV and VH return.

In this paper, we study the complete polarimetric signatures of a canopy of dielectric cylinders overlying a homogeneous half space with the first and second order solutions of the vector radiative transfer theory. The energy conservation issue is addressed by calculating the elements of the extinction matrix and the elements of the phase matrix in a manner that is consistent with energy conservation. Two methods are used. In the first method, the surface fields and the internal fields of the dielectric cylinder are calculated by using the fields of an infinite cylinder [4]. We calculate the extinction matrix, however, by summing the absorption and scattering to ensure energy conservation. In the second method, the method of moments [21–22], which is a numerical solution of Maxwell's equations, is used to calculate the elements of the extinction and phase matrices. Results of the computed Mueller matrices from the two methods are tabulated and compared. The CPU for the two methods and for first and second order solutions of the transfer theory are compared and discussed. The computation based on method of moments is not formidable compared with the infinite cylinder approach because much of the CPU in transfer theory is consumed on averaging over orientations and integration over directions in second order theory. The polarimetric signatures, copolarized and depolarized return, degree of polarization, and phase differences are studied as a function of the orientation, sizes, and dielectric properties of the cylinders using parameters of vegetation canopy overlying the ground [23–25]. Salient features of the numerical results are as follows. (1) The infinite cylinder approximation gives reasonable approximations for cylinders of small radius and deviate from MOM for larger radius. (2) The infinite cylinder approximation also violates reciprocity and can give significantly different results for HV and HV returns, particularly for problems of larger radius. (3) In scattering by vegetation canopy, second order scattering effects can become important for frequencies around C-band and higher. For some medium parameters, second order scattering can also be important at L-band.

The numerical computation in this paper is intensive. However, it can be used to provide training data for neural network which can be used for speedy inversion of parameters from remote sensing data [26]. Polarimetric sensing utilizing complete Mueller matrix is an important remote sensing tool. Recently, it has also been shown that the third and fourth Stokes parameters can be nonzero in passive remote sensing so that complete polarimetric passive remote sensing is also possible [27].

II. FIRST AND SECOND ORDER SOLUTIONS OF THE VECTOR RADIATIVE TRANSFER EQUATION FOR A LAYER OF SPARSELY DISTRIBUTED NONSPHERICAL PARTICLES

Consider a collection of sparsely distributed nonspherical particles with permittivity ϵ_s embedded in a background medium with permittivity ϵ (region 1) overlying a homogeneous half space of dielectric of permittivity ϵ_2 (region 2). An incident wave is launched from region 0 in direction $(\pi - \theta_0, \phi_0)$. The permittivity of region 0 is the same as that of the background medium of region 1. The vector radiative

transfer equation in region 1 is of the following form, with $0 \le \theta \le \pi, 0 \le \phi \le 2\pi$.

$$\cos\theta \frac{d}{dz}\overline{I}(\theta,\phi,z) = -\overline{\overline{\kappa}}_e(\theta,\phi)\cdot\overline{I}(\theta,\phi,z) + \int_0^{2\pi} d\phi' \int_0^{\pi} d\theta' \sin\theta' \,\overline{\overline{P}}(\theta,\phi;\theta',\phi)\cdot\overline{I}(\theta',\phi',z) \quad (1)$$

where $\overline{I}(\theta,\phi,z)$ is a 4×1 column vector denoting the modified Stokes parameters in direction (θ,ϕ)

$$\overline{I}(\theta,\phi,z) = \begin{bmatrix} I_v \\ I_h \\ U \\ V \end{bmatrix} \quad (2)$$

$\overline{\overline{\kappa}}_e(\theta,\phi)$ is a 4×4 extinction matrix given by

$$\overline{\overline{\kappa}}_e(\theta,\phi) = \frac{2\pi n_0}{k} \begin{bmatrix} 2\mathrm{Im}<f_{vv}> & 0 & \mathrm{Im}<f_{vh}> & -\mathrm{Re}<f_{vh}> \\ 0 & 2\mathrm{Im}<f_{hh}> & \mathrm{Im}<f_{hv}> & \mathrm{Re}<f_{hv}> \\ 2\mathrm{Im}<f_{hv}> & 2\mathrm{Im}<f_{vh}> & \mathrm{Im}<f_{vv}+f_{hh}> & \mathrm{Re}<f_{vv}-f_{hh}> \\ 2\mathrm{Re}<f_{hv}> & -2\mathrm{Re}<f_{vh}> & \mathrm{Re}<f_{hh}-f_{vv}> & \mathrm{Im}<f_{vv}+f_{hh}> \end{bmatrix} \quad (3)$$

where n_0 is the number of particles per unit volume. In (3), all the f_{jm}, $j,m = v,h$ are forward scattering amplitudes from (θ,ϕ) of polarization m into the same direction (θ,ϕ) of polarization j. The phase matrix $\overline{\overline{P}}(\theta,\phi;\theta',\phi')$ is a 4×4 matrix and is given by

$$\overline{\overline{P}}(\theta,\phi;\theta',\phi') = n_0 \begin{bmatrix} <|f_{vv}|^2> & <|f_{vh}|^2> & \mathrm{Re}<f_{vv}f_{vh}^*> & -\mathrm{Im}<f_{vv}f_{vh}^*> \\ <|f_{hv}|^2> & <|f_{hh}|^2> & \mathrm{Re}<f_{hv}f_{hh}^*> & -\mathrm{Im}<f_{hv}f_{hh}^*> \\ 2\mathrm{Re}<f_{vv}f_{hv}^*> & 2\mathrm{Re}<f_{vh}f_{hh}^*> & \mathrm{Re}<f_{vv}f_{hh}^*+f_{vh}f_{hv}^*> & -\mathrm{Im}<f_{vv}f_{hh}^*-f_{vh}f_{hv}^*> \\ 2\mathrm{Im}<f_{vv}f_{hv}^*> & 2\mathrm{Im}<f_{vh}f_{hh}^*> & \mathrm{Im}<f_{vv}f_{hh}^*+f_{vh}f_{hv}^*> & \mathrm{Re}<f_{vv}f_{hh}^*-f_{vh}f_{hv}^*> \end{bmatrix} \quad (4)$$

In (4), all the f_{jm}, $j,m = v,h$ are bistatic scattering amplitudes denoting scattering from a general direction (θ',ϕ') of polarization m into direction (θ,ϕ) of

polarization j. In (1), we can distinguish between the upward going Stokes vector in direction (θ,ϕ) and the downward going Stokes vector in direction $(\pi-\theta,\phi)$ by considering the range $0 \le \theta \le \pi/2$ and $0 \le \phi \le 2\pi$. The boundary conditions for the vector radiative transfer equation assuming a smooth boundary at $z = -d$ are as follows. At $z = 0$, and at $z = d$, the boundary conditions are respectively

$$\overline{I}(\pi-\theta,\phi,z=0) = \overline{I}_0\,\delta(\cos\theta-\cos\theta_0)\,\delta(\phi-\phi_0) \quad (5)$$

$$\overline{I}(\theta,\phi,z=-d) = \overline{\overline{R}}(\theta)\cdot\overline{I}(\pi-\theta,\phi,z=-d) \quad (6)$$

for $0 \le \theta \le \pi/2$. In (5) and (6), $\overline{I}_0$ is the incident Stokes vector, $\overline{\overline{R}}(\theta)$ is the 4×4 reflectivity matrix for the interface separating regions 1 and 2 and is given by

$$\overline{\overline{R}}(\theta) = \begin{bmatrix} |R_v(\theta)|^2 & 0 & 0 & 0 \\ 0 & |R_h(\theta)|^2 & 0 & 0 \\ 0 & 0 & \mathrm{Re}(R_v(\theta)R_h(\theta)^*) & -\mathrm{Im}(R_v(\theta)R_h(\theta)^*) \\ 0 & 0 & \mathrm{Im}(R_v(\theta)R_h(\theta)^*) & \mathrm{Re}(R_v(\theta)R_h(\theta)^*) \end{bmatrix} \quad (7)$$

where $R_v(\theta)$ and $R_h(\theta)$ are respectively the Fresnel reflection coefficients for vertically and horizontally polarized waves. Given the vector radiative transfer equation (1) and the boundary conditions in (5) and (6), the Stokes vector can be calculated either numerically or iteratively. Once that is solved, the overall scattered Stokes vector in direction (θ_s,ϕ_s) that is observed by the receiver is $I_s(\theta_s,\phi_s) = I(\theta_s,\phi_s,z=0) = [I_{vs},I_{hs},U_s,V_s]$ and can be calculated. It is proportional to $\overline{I}_0$ with the proportionality represented by the 4×4 averaged Mueller matrix $\overline{\overline{M}}(\theta_s,\phi_s;\pi-\theta_0,\phi_0)$ as follows

$$\overline{I}_s(\theta_s,\phi_s) = \overline{\overline{M}}(\theta_s,\phi_s;\pi-\theta_0,\phi_0)\cdot\overline{I}_0 \quad (8)$$

The Mueller matrix represents the overall polarimetric characteristics of the layer of random discrete scatterers including all multiple scattering effects and boundary reflections that are included in the vector radiative transfer theory. In this paper, the results based on the Mueller matrix will be illustrated for the backscattering direction with $\theta_s = \theta_0$ and $\phi_s = \pi+\phi_0$. Based on the Mueller matrix, we shall illustrate four polarimetric signatures: the phase difference, the copolarized return, the depolarized return, and the degree of polarization. The phase difference between vv and hh waves, ϕ_{vh}, (actually the phase at which the probability density function of phase difference is maximum [28]) is

$$\phi_{vh} = \tan^{-1}\left(\frac{M_{43}-M_{34}}{M_{33}+M_{44}}\right) \quad (9)$$

where M_{ij} is the ij element of the Mueller matrix. For a completely polarized incident wave, with ellipticity angle χ, $-45^\circ \le \chi \le 45^\circ$ and orientation angle $\Psi, 0^\circ \le \Psi \le 180^\circ$, the incident Stokes vector with unit total intensity is defined

by

$$\bar{I}_0 = \begin{bmatrix} \dfrac{1-\cos 2\chi\cos 2\Psi}{2} \\ \dfrac{1+\cos 2\chi\cos 2\Psi}{2} \\ -\cos 2\chi\sin 2\Psi \\ \sin 2\chi \end{bmatrix} \tag{10}$$

where the orientation angle Ψ is defined as the angle between the major axis of the ellipse and the direction of horizontal polarization. The normalized copolarized received power P_n in the backscattering direction corresponds to the case when the receiving antenna measures the same polarization as that of the transmitting antenna. The copolarized power P_n and the backscattering co-polarized coefficient σ are, respectively,

$$P_n = \frac{I_{vs}}{2}(1-\cos 2\chi\cos 2\Psi) + \frac{I_{hs}}{2}(1+\cos 2\chi\cos 2\Psi) + \frac{U_s}{2}\cos 2\chi\sin 2\Psi + \frac{V_s}{2}\sin 2\chi \tag{11}$$

$$\sigma = 4\pi\cos\theta_0 P_n \tag{12}$$

The depolarized power P_d and the depolarized coefficient σ_d are respectively

$$P_d = I_{vs} + I_{hs} - P_n \tag{13}$$

$$\sigma_d = 4\pi\cos\theta_0 P_d \tag{14}$$

The degree of polarization for the scattered Stokes vector is

$$m_s = \frac{\sqrt{Q_s^2 + U_s^2 + V_s^2}}{I_s} \tag{15}$$

where $Q_s = I_{vs} - I_{hs}$ and $I_s = I_{vs} + I_{hs}$.

In the following we list the second order theory of the vector radiative transfer equation. To reduce the complexity, we adopt the viewpoint by regarding a volume scattering as an order of scattering and a boundary reflection as half an order of scattering [15]. In this manner, the second order theory will include only five terms: (a) a single upward scattering by the particles, (b) a downward single scattering by the particles that is followed by a reflection off the boundary at $z = -d$, (c) a reflection by the boundary that is followed by a single upward scattering by the particles , (d) a reflection by the boundary at $z = -d$, followed by a single downward scattering by the particles and further followed by a reflection off the boundary at $z = -d$, which then proceeds upward to the receiver, and (e) double volume scattering [12]. The sum of (a), (b), (c), and (d) shall be labelled as first order theory and the sum of all five terms shall be labelled as second order theory.

$$\begin{aligned}
&M_{mj}(\theta,\phi;\pi-\theta_0,\phi_0) \\
&= \sec\theta \sum_{k,i} \overline{\overline{E}}_{mk}(\theta,\phi)\left\{\overline{\overline{E}}(\theta,\phi)^{-1}\overline{\overline{P}}(\theta,\phi;\pi-\theta_0,\phi_0)\overline{\overline{E}}(\pi-\theta_0,\phi_0)\right\}_{ki} \\
&\times \frac{1-e^{-\beta_k(\theta,\phi)d\sec\theta-\beta_i(\pi-\theta_0,\phi_0)d\sec\theta_0}}{\beta_k(\theta,\phi)\sec\theta+\beta_i(\pi-\theta_0,\phi_0)\sec\theta_0}\left\{\overline{\overline{E}}(\pi-\theta_0,\phi_0)^{-1}\right\}_{ij} \\
&+ \sum_{k,i}\sec\theta\left\{\overline{\overline{E}}(\theta,\phi)\overline{\overline{D}}(-\beta(\theta,\phi)d\sec\theta)\overline{\overline{E}}(\theta,\phi)^{-1}\overline{\overline{R}}(\theta)\overline{\overline{E}}(\pi-\theta,\phi)\right\}_{mk} \\
&\times\left\{\overline{\overline{E}}(\pi-\theta,\phi)^{-1}\overline{\overline{P}}(\pi-\theta,\phi;\pi-\theta_0,\phi_0)\overline{\overline{E}}(\pi-\theta_0,\phi_0)\right\}_{ki} \\
&\times \frac{e^{-\beta_k(\pi-\theta,\phi)d\sec\theta}-e^{-\beta_i(\pi-\theta_0,\phi_0)d\sec\theta_0}}{\beta_i(\pi-\theta_0,\phi_0)\sec\theta_0-\beta_k(\pi-\theta,\phi)\sec\theta}\left\{\overline{\overline{E}}(\pi-\theta_0,\phi_0)^{-1}\right\}_{ij} \\
&+\sec\theta\sum_{k,i}\overline{\overline{E}}_{mk}(\theta,\phi)\left\{\overline{\overline{E}}(\theta,\phi)^{-1}\overline{\overline{P}}(\theta,\phi;\theta_0,\phi_0)\overline{\overline{E}}(\theta_0,\phi_0)\right\}_{ki} \\
&\times \frac{e^{-\beta_k(\theta,\phi)d\sec\theta}-e^{-\beta_i(\theta_0,\phi_0)d\sec\theta_0}}{\beta_i(\theta_0,\phi_0)\sec\theta_0-\beta_k(\theta,\phi)\sec\theta}\left\{\overline{\overline{E}}(\theta_0,\phi_0)^{-1}\overline{\overline{R}}(\theta_0)\overline{\overline{E}}(\pi-\theta_0,\phi_0)\right. \\
&\left.\cdot\overline{\overline{D}}(-\beta(\pi-\theta_0,\phi_0)d\sec\theta_0)\overline{\overline{E}}(\pi-\theta_0,\phi_0)^{-1}\right\}_{ij} \\
&+\sum_{k,i}\sec\theta\left\{\overline{\overline{E}}(\theta,\phi)\overline{\overline{D}}(-\beta(\theta,\phi)d\sec\theta)\overline{\overline{E}}(\theta,\phi)^{-1}\overline{\overline{R}}(\theta)\overline{\overline{E}}(\pi-\theta,\phi)\right\}_{mk} \\
&\times\left\{\overline{\overline{E}}(\pi-\theta,\phi)^{-1}\overline{\overline{P}}(\pi-\theta,\phi;\theta_0,\phi_0)\overline{\overline{E}}(\theta_0,\phi_0)\right\}_{ki} \\
&\times \frac{1-e^{-\beta_k(\pi-\theta,\phi)d\sec\theta-\beta_i(\theta_0,\phi_0)d\sec\theta_0}}{\beta_k(\pi-\theta,\phi)\sec\theta+\beta_i(\theta_0,\phi_0)\sec\theta_0}\left\{\overline{\overline{E}}(\theta_0,\phi_0)^{-1}\overline{\overline{R}}(\theta_0)\overline{\overline{E}}(\pi-\theta_0,\phi_0)\right. \\
&\left.\cdot\overline{\overline{D}}(-\beta(\pi-\theta_0,\phi_0)d\sec\theta_0)\overline{\overline{E}}(\pi-\theta_0,\phi_0)^{-1}\right\}_{ij} \\
&+\int_0^{2\pi}d\phi'\int_0^{\frac{\pi}{2}}d\theta'\sin\theta'\sum_{n,k,i}\overline{\overline{E}}_{mn}(\theta,\phi)\left(\overline{\overline{E}}(\pi-\theta_0,\phi_0)^{-1}\right)_{ij} \\
&\times\left\{\left[\cos\theta_0\frac{1-e^{-\beta_n(\theta,\phi)d\sec\theta-\beta_i(\pi-\theta_0,\phi_0)d\sec\theta_0}}{\beta_n(\theta,\phi)\cos\theta_0+\beta_i(\pi-\theta_0,\phi_0)\cos\theta}\right.\right.
\end{aligned}$$

$$
- \cos\theta' \frac{\left(e^{-\beta_k(\theta',\phi')d\sec\theta'} - e^{-\beta_n(\theta,\phi)d\sec\theta}\right) e^{-\beta_i(\pi-\theta_0,\phi_0)d\sec\theta_0}}{\beta_n(\theta,\phi)\cos\theta' - \beta_k(\theta',\phi')\cos\theta}\Bigg]
$$

$$
\times \frac{\cos\theta_0}{\beta_k(\theta',\phi')\cos\theta_0 + \beta_i(\pi-\theta_0,\phi_0)\cos\theta'}
$$

$$
\times \left[\overline{\overline{E}}(\theta,\phi)^{-1}\overline{\overline{P}}(\theta,\phi;\theta',\phi')\overline{\overline{E}}(\theta',\phi')\right]_{nk}
$$

$$
\times \left[\overline{\overline{E}}(\theta',\phi')^{-1}\overline{\overline{P}}(\theta',\phi';\pi-\theta_0,\phi_0)\overline{\overline{E}}(\pi-\theta_0,\phi_0)\right]_{ki}
$$

$$
+ \frac{\cos\theta_0}{[\beta_n(\theta,\phi)\cos\theta' + \beta_k(\pi-\theta',\phi')\cos\theta]\,[\beta_n(\theta,\phi)\cos\theta_0 + \beta_i(\pi-\theta_0,\phi_0)\cos\theta]}
$$

$$
\times \Bigg[\cos\theta + \frac{e^{-\beta_n(\theta,\phi)d\sec\theta}}{\beta_i(\pi-\theta_0,\phi_0)\cos\theta' - \beta_k(\pi-\theta',\phi')\cos\theta_0}
$$

$$
\times \Big\{\beta_n(\theta,\phi)\cos\theta_0\cos\theta'\left(e^{-\beta_i(\pi-\theta_0,\phi_0)d\sec\theta_0} - e^{-\beta_k(\pi-\theta',\phi')d\sec\theta'}\right)
$$

$$
+ \cos\theta\Big[\cos\theta_0\beta_k(\pi-\theta',\phi')e^{-\beta_i(\pi-\theta_0,\phi_0)d\sec\theta_0}
$$

$$
- \cos\theta'\beta_i(\pi-\theta_0,\phi_0)e^{-\beta_k(\pi-\theta',\phi')d\sec\theta'}\Big]\Big\}\Bigg]
$$

$$
\times \left[\overline{\overline{E}}(\theta,\phi)^{-1}\overline{\overline{P}}(\theta,\phi;\pi-\theta',\phi')\overline{\overline{E}}(\pi-\theta',\phi')\right]_{nk}
$$

$$
\times \left\{\overline{\overline{E}}(\pi-\theta',\phi')^{-1}\overline{\overline{P}}(\pi-\theta',\phi';\pi-\theta_0,\phi_0)\overline{\overline{E}}(\pi-\theta_0,\phi_0)\right\}_{ki}\Bigg\} \tag{16}
$$

where $D(\beta(\theta,\phi)z\sec\theta)$ is a 4×4 diagonal matrix with the ith element equal to $\exp(\beta_i(\theta,\phi)z\sec\theta)$.

In (16), $\overline{\overline{E}}(\theta,\phi)$ is the eigenmatrix for coherent propagation and $\beta_i, i=1,2,3,4$, are the eigenvalues of coherent wave propagation [2,11,15]. In the numerical examples of this paper, we shall only consider the statistical azimuthal symmetric case when the vertical polarized waves and the horizontal polarized waves are the characteristic polarizations of the medium. In this case, we have [2,11,15],

$$
\overline{\overline{E}}(\theta,\phi) = \begin{bmatrix} 1 & 0 & 0 & 0 \\ 0 & 1 & 0 & 0 \\ 0 & 0 & 1 & 1 \\ 0 & 0 & i & -i \end{bmatrix} \tag{17}
$$

$$
\overline{\overline{\beta}}(\theta,\phi) = \begin{bmatrix} \beta_1(\theta,\phi) \\ \beta_2(\theta,\phi) \\ \beta_3(\theta,\phi) \\ \beta_4(\theta,\phi) \end{bmatrix} = \frac{2\pi n_0}{k} \begin{bmatrix} 2 < \mathrm{Im} f_{vv}(\theta,\phi;\theta,\phi) > \\ 2 < \mathrm{Im} f_{hh}(\theta,\phi;\theta,\phi) > \\ i(< f^*_{vv}(\theta,\phi;\theta,\phi) - f_{hh}(\theta,\phi;\theta,\phi) >) \\ i(< f^*_{hh}(\theta,\phi;\theta,\phi) - f_{vv}(\theta,\phi;\theta,\phi) >) \end{bmatrix} \tag{18}
$$

III. CALCULATION OF EXTINCTION MATRIX ELEMENTS TO ENSURE ENERGY CONSERVATION

The vector radiative transfer equations as given in equations (1), (3)–(4) obey energy conservation if exact numerical calculations are made in calculating the scattering amplitudes to be used in the extinction matrix and phase matrix. If approximate solutions are used to calculate the scattering amplitudes, e.g. Rayleigh scattering approximation and infinite cylinder approximation, steps need to be taken to ensure that the extinction matrix elements and the phase matrix elements are consistent with energy conservation. In this case, we calculate the real part of the forward scattering amplitudes by using the approximate expressions of the forward scattering amplitudes. However, the imaginary parts of the forward scattering amplitudes are calculated as follows. Consider a plane wave with angular frequency ω incident in the direction $\hat{s}$ onto the particle. The particle has permittivity ϵ_p and is occupying volume V_p. The incident field has the electric vector given by $\hat{v}_i E_v + \hat{h}_i E_h$. Then, following a procedure similar to the derivation of the optical theorem except using a linear combination of the two polarizations [2], we get

$$
\begin{aligned}
&\frac{4\pi}{k}\Big\{\mathrm{Im}\left(f_{vv}(\hat{s},\hat{s})\right)|E_v|^2 + \mathrm{Im}\left(f_{hh}(\hat{s},\hat{s})\right)|E_h|^2 \\
&\qquad - \mathrm{Im}\left[\left(f^*_{vh}(\hat{s},\hat{s}) - f_{hv}(\hat{s},\hat{s})\right)E_v E^*_h\right]\Big\} \\
&= \eta\int_{V_p} d\bar{r}'\,\omega\epsilon''_p\left|\overline{E}_p(\bar{r}')\right|^2 + \int_{4\pi} d\hat{s}'\Big[\left|f_{vv}(\hat{s}',\hat{s})E_v + f_{vh}(\hat{s}',\hat{s})E_h\right|^2 \\
&\qquad + \left|f_{hv}(\hat{s}',\hat{s})E_v + f_{hh}(\hat{s}',\hat{s})E_h\right|^2\Big]
\end{aligned} \tag{19}
$$

where η is the wave impedance of the background medium, ϵ''_p is the imaginary part of the permittivity of the particle, and $\overline{E}_p(r')$ is the field inside the particle.

Next, consider the incident wave to be of unit amplitude in the vertical polarization, i.e., $E_v = 1$ and $E_h = 0$. We then calculate the interior field of the particle $\overline{E}^v_p(r')$ and then the imaginary part of the forward scattering amplitude $\mathrm{Im} f_{vv}$ is given by (20) below. In the second case, consider the incident wave to be of unit amplitude in the horizontal polarization, i.e., $E_v = 0$ and $E_h = 1$. We then calculate the interior field of the particle $\overline{E}^h_p(r')$ and then the imaginary

part of the forward scattering amplitude $\mathrm{Im} f_{hh}$ is given by (21) below

$$\frac{4\pi}{k}\mathrm{Im} f_{vv}(\hat{s},\hat{s}) = \eta\int_{V_p} d\bar{r}'\omega\epsilon_p''\left|E_p^V(r')\right|^2 + \int_{4\pi} d\hat{s}'\left[\left|f_{vv}(\hat{s}',\hat{s})\right|^2 + \left|f_{hv}(\hat{s}',\hat{s})\right|^2\right] \tag{20}$$

$$\frac{4\pi}{k}\mathrm{Im} f_{hh}(\hat{s},\hat{s}) = \eta\int_{V_p} d\bar{r}'\omega\epsilon_p''\left|E_p^H(r')\right|^2 + \int_{4\pi} d\hat{s}'\left[\left|f_{vh}(\hat{s}',\hat{s})\right|^2 + \left|f_{hh}(\hat{s}',\hat{s})\right|^2\right] \tag{21}$$

Thus, to use (20) and (21) to calculate the imaginary part of the forward scattering amplitudes, we have to first obtain the internal fields and then integrate over the volume of the particle. To calculate $\mathrm{Im} f_{vh}$ and $\mathrm{Im} f_{hv}$, we consider an incident linear polarization L with

$$E_v = E_h = \frac{1}{\sqrt{2}} \tag{22}$$

and the internal field represented by $\overline{E}_p^L(r')$ in this case. Then

$$\begin{aligned}&\frac{2\pi}{k}\mathrm{Im}\left\{\left(f_{vv}(\hat{s},\hat{s})\right) + \mathrm{Im}\left(f_{hh}(\hat{s},\hat{s})\right) - \mathrm{Im}\left[\left(f_{vh}^*(\hat{s},\hat{s}) - f_{hv}(\hat{s},\hat{s})\right)\right]\right\}\\ &=\eta\int_{V_p} d\bar{r}'\omega\epsilon_p''\left|\overline{E}_p^L(\bar{r}')\right|^2 + \frac{1}{2}\int_{4\pi} d\hat{s}'\left[\left|f_{vv}(\hat{s}',\hat{s}) + f_{vh}(\hat{s}',\hat{s})\right|^2\right.\\ &\quad\left.+\left|f_{hv}(\hat{s}',\hat{s}) + f_{hh}(\hat{s}',\hat{s})\right|^2\right]\end{aligned} \tag{23}$$

In general, we cannot separate $\mathrm{Im} f_{vh}$ and $\mathrm{Im} f_{hv}$ in (23). We can, however, separate them by assuming inversion symmetry of the particle. If the particle obeys inversion symmetry, we have a relation between f_{vh} and f_{hv}. Furthermore, we have a reciprocal relation between f_{vh} and f_{hv} [2,27]. The reciprocal relations and the inversion symmetry relations are given respectively in (24) and (25).

$$f_{vh}(\hat{s}',\hat{s}) = -f_{hv}(-\hat{s},-\hat{s}') \tag{24}$$

$$f_{hv}(\hat{s}',\hat{s}) = -f_{hv}(-\hat{s}',-\hat{s}) \tag{25}$$

Combining (23), (24), and (25) gives

$$f_{vh}(\hat{s},\hat{s}) = f_{hv}(\hat{s},\hat{s}) \tag{26}$$

$$\begin{aligned}\frac{4\pi}{k}\mathrm{Im}\left(f_{hv}(\hat{s},\hat{s})\right) &= \frac{4\pi}{k}\mathrm{Im}\left(f_{vh}(\hat{s},\hat{s})\right)\\ &=\eta\int_{V_p} d\bar{r}'\omega\epsilon_p''\left|\overline{E}_p^L(\bar{r}')\right|^2 + \frac{1}{2}\int_{4\pi} d\hat{s}'\left[\left|f_{vv}(\hat{s}',\hat{s}) + f_{vh}(\hat{s}',\hat{s})\right|^2\right.\\ &\quad\left.+\left|f_{hv}(\hat{s}',\hat{s}) + f_{hh}(\hat{s}',\hat{s})\right|^2\right]\\ &\quad - \frac{2\pi}{k}\left\{\mathrm{Im}\left(f_{vv}(\hat{s},\hat{s})\right) + \mathrm{Im}\left(f_{hh}(\hat{s},\hat{s})\right)\right\}\end{aligned} \tag{27}$$

Thus the imaginary parts of the forward scattering amplitudes can be calculated by using (20), (21), and (27). Equation (27), however, only applies if the particle has inversion symmetry.

IV. SCATTERING AMPLITUDES AND EXTINCTION MATRIX ELEMENTS OF A FINITE DIELECTRIC CYLINDER BASED ON INFINITE CYLINDER APPROXIMATION

In this section, we derive expressions for the scattering amplitudes for a finite cylinder of length L, radius a, permittivity ϵ_p, and wavenumber k_p. The surface field on the surface of the finite length cylinder is assumed to be the same as that of an infinite cylinder. Huygen's principle is then used to calculate the scattering amplitude functions. The radiation from the two end faces of the cylinder are ignored. There are two choices of the surface fields in applying Huygen's principle. One choice is to use the total surface field which is the sum of the incident field and the scattered field [4,13]. The second choice is to use only the scattered field for the surface field. The second choice has the advantage that the scattered field from the finite cylinder will vanish in the event that the permittivity ϵ_p approaches the value of the background permittivity ϵ. In this section, we also derive expressions for the absorption of the cylinder to calculate the imaginary parts of the forward scattering amplitudes in a manner consistent with energy conservation. In the derivation of the absorption, we also assume that the interior field of the finite cylinder is the same as that of an infinite cylinder and integration is performed over the volume of the finite cylinder.

Consider an incident plane wave in the direction $\hat{s}_i$ impinging on the cylinder with axis $\hat{z}_b$ (Fig. 2). The subscript b denotes body frame with $\hat{x}_b$, $\hat{y}_b$, and $\hat{z}_b$ as axes. The axis of symmetry $\hat{z}_b$ is at an angle with respect to the principal frame of Fig. 1.

$$\hat{z}_b = \sin\beta\cos\alpha\,\hat{x} + \sin\beta\sin\alpha\,\hat{y} + \cos\beta\,\hat{z} \tag{28}$$

Note that the results in this section are calculated for one cylinder with fixed orientation as represented by α and β. The results will be averaged over the orientation in Section VI. Let the incident electric field be given by

$$\overline{E}^i = \left(E_{vbi}\,\hat{v}_{bi} + E_{hbi}\,\hat{h}_{bi}\right) \tag{29}$$

$$\hat{s}_i = \sin\theta_{bi}\,\hat{x}_b + \cos\theta_{bi}\,\hat{z}_b \tag{30}$$

$$\hat{v}_{bi} = \cos\theta_{bi}\,\hat{x}_b - \sin\theta_{bi}\,\hat{z}_b \tag{31}$$

$$\hat{h}_{bi} = \hat{y}_b \tag{32}$$

Since the cylinder is rotationally symmetric, we have chosen $\hat{y}_b$ to coincide with $\hat{h}_{bi}$ without loss of generality. In (29), without loss of generality, we have let the incident direction to be in the $\hat{z}_b\hat{x}_b$ plane. We assume the surface fields of the finite cylinder to be the same as that of an infinite cylinder and the surface fields can be expressed as follows

$$\begin{bmatrix} E_{\phi b}\\ E_{zb}\\ \eta H_{\phi b}\\ \eta H_{zb}\end{bmatrix} = \sum_{m=-\infty}^{\infty} e^{im\phi_b + ik_{zbi}z_b}\begin{bmatrix} E_{\phi m}\\ E_{zm}\\ \eta H_{\phi m}\\ \eta H_{zm}\end{bmatrix} \tag{33}$$

where

$$k_{zbi} = k\cos\theta_{bi} \tag{34}$$

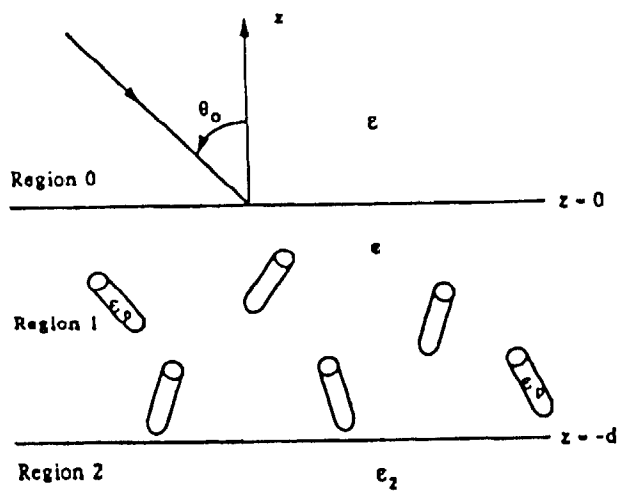

Figure 1. An incident plane wave impinging upon a layer of sparsely distributed dielectric cylinders of finite length and permittivity ε_p. The background permittivity of the layer is ε and is the same as region 0. The layer is overlying a homogeneous half space with permittivity ε_2.

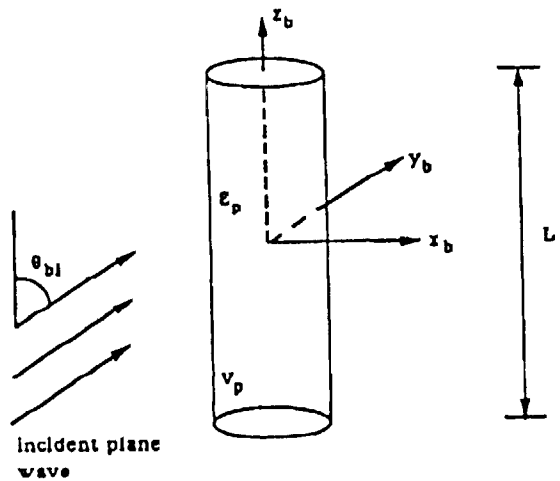

Figure 2. The dielectric cylinder with permittivity ε_p in its body frame with axes x_b, y_b, and symmetry axis z_b. The length is L and the radius is a. The incident plane wave is launched in the direction $(\theta_{bi}, \phi_{bi} = 0)$.

The surface fields based on the total field approach and the scattered field can be expressed in terms of the coefficients C_m and ηD_m which are governed by the following equations.

$$C_m J_m(w_p)\left(k_p^2a^2 - k^2a^2\right)\frac{mk_{zbi}a}{w_p^2} + \eta D_m ika\left[-\frac{w^2 J_m'(w_p)}{w_p} + \frac{J_m(w_p)wH_m'(w)}{H_m(w)}\right] = -\frac{2E_{hbi}w}{\pi H_m(w)} \tag{35}$$

$$C_m ika\left[\frac{\varepsilon_p}{\varepsilon}\frac{w^2 J_m'(w_p)}{w_p} - \frac{J_m(w_p)wH_m'(w)}{H_m(w)}\right] + \eta D_m J_m(w_p)\left(k_p^2a^2 - k^2a^2\right)\frac{mk_{zbi}a}{w_p^2} = -\frac{2E_{vbi}w}{\pi H_m(w)} \tag{36}$$

where

$$w = ka\sin\theta_{bi} \tag{37}$$

$$w_p = \sqrt{k_p^2 - k^2\cos^2\theta_{bi}}\,a \tag{38}$$

k_p is the wavenumber of the particle, J_m and H_m are, respectively, the Bessel function and Hankel function of the first kind. In the following we list the two approximations.

(1) The scattered field approximation. The surface tangential fields are replaced by that of the scattered field. Thus we use the following substitution for (33)

$$\begin{bmatrix} E_{\phi m} \\ E_{zm} \\ \eta H_{\phi m} \\ \eta H_{zm} \end{bmatrix} = \begin{bmatrix} E^s_{\phi m} \\ E^s_{zm} \\ \eta H^s_{\phi m} \\ \eta H^s_{zm} \end{bmatrix} \tag{39}$$

where

$$E^s_{\phi m} = i^m\left(-\frac{mk_{zbi}a}{w^2}A_m H_m(w) - \frac{ika}{w}\eta B_m H_m'(w)\right) \tag{40}$$

$$E^s_{zm} = i^m A_m H_m(w) \tag{41}$$

$$\eta H^s_{\phi m} = i^m\left(-\frac{mk_{zbi}a}{w^2}\eta B_m H_m(w) + \frac{ika}{w}A_m H_m'(w)\right) \tag{42}$$

$$\eta H^s_{zm} = i^m \eta B_m H_m(w) \tag{43}$$

$$A_m = \frac{C_m J_m(w_p)}{H_m(w)} + E_{vbi}\sin\theta_{bi}\frac{J_m(w)}{H_m(w)} \tag{44}$$

$$\eta B_m = \eta D_m\frac{J_m(w_p)}{H_m(w)} - E_{hbi}\sin\theta_{bi}\frac{J_m(w)}{H_m(w)} \tag{45}$$

(2) The total field approximation. In this case the surface field harmonics are approximated by the total field on the surface of the infinite cylinder. The total field

is the sum of the scattered field and incident field. Thus, in this approximation, we use the following substitution for (33)

$$E_{\phi m} = E^s_{\phi m} + i^m \left(E_{vbi} \cos\theta_{bi} \frac{m J_m(w)}{w} - i E_{hbi} J'_m(w) \right) \tag{46}$$

$$E_{zm} = E^s_{zm} - i^m E_{vbi} \sin\theta_{bi} J_m(w) \tag{47}$$

$$\eta H_{\phi m} = \eta H^s_{\phi m} + i^m \left(-E_{hbi} \cos\theta_{bi} \frac{m J_m(w)}{w} - i E_{vbi} J'_m(w) \right) \tag{48}$$

$$\eta H_{zm} = \eta H^s_{zm} + i^m E_{hbi} \sin\theta_{bi} J_m(w) \tag{49}$$

Given the surface fields of either (1) scattered fields or (2) total fields, the scattering amplitudes in the body frame are

$$f_{v_b\alpha}(\theta_{bs}, \phi_{bs}; \theta_{bi}, \phi_{bi} = 0) = a \frac{\sin\left(k \frac{L}{2}(\cos\theta_{bs} - \cos\theta_{bi})\right)}{k(\cos\theta_{bs} - \cos\theta_{bi})} \sum_{m=-\infty}^{\infty} (-i)^m e^{im\phi_{bs}} F_{v_b m} \tag{50a}$$

$$f_{h_b\alpha}(\theta_{bs}, \phi_{bs}; \theta_{bi}, \phi_{bi} = 0) = a \frac{\sin\left(k \frac{L}{2}(\cos\theta_{bs} - \cos\theta_{bi})\right)}{k(\cos\theta_{bs} - \cos\theta_{bi})} \sum_{m=-\infty}^{\infty} (-i)^m e^{im\phi_{bs}} F_{h_b m}. \tag{50b}$$

where

$$F_{v_b m} = -ik \sin\theta_{bs} \eta H_{\phi m} J_m(w_s) - \frac{m}{w_s} \cos\theta_{bs} \eta H_{zm} J_m(w_s) - k E_{zm} J'_m(w_s) \tag{51a}$$

$$F_{h_b m} = -ik \sin\theta_{bs} E_{\phi m} J_m(w_s) - \frac{m}{w_s} \cos\theta_{bs} E_{zm} J_m(w_s) + k\eta H_{zm} J'_m(w_s) \tag{51b}$$

and $\alpha = v_b,\ h_b$. In (50)–(51), when we set $\alpha = v_b$, we let ($E_{vbi} = 1,\ E_{hbi} = 0$) in (35)–(36) and (47)–(49) so that the incident wave is vertically polarized in the body frame. When we set $\alpha = h_b$ in (50)–(51), we let ($E_{vbi} = 0,\ E_{hbi} = 1$) in (35)–(36) and (47)–(49) so that the incident wave is horizontally polarized in the body frame. To transform between the body frame to the principal frame, we use the following 2×2 matrix multiplication

$$\begin{bmatrix} f_{vv}(\theta_s, \phi_s; \theta_i, \phi_i) & f_{vh}(\theta_s, \phi_s; \theta_i, \phi_i) \\ f_{hv}(\theta_s, \phi_s; \theta_i, \phi_i) & f_{hh}(\theta_s, \phi_s; \theta_i, \phi_i) \end{bmatrix} = \begin{bmatrix} \hat{v}_s \cdot \hat{v}_{bs} & \hat{v}_s \cdot \hat{h}_{bs} \\ \hat{h}_s \cdot \hat{v}_{bs} & \hat{h}_s \cdot \hat{h}_{bs} \end{bmatrix}$$

$$\times \begin{bmatrix} f_{v_b v_b}(\theta_{bs}, \phi_{bs}; \theta_{bi}, \phi_{bi} = 0) & f_{v_b h_b}(\theta_{bs}, \phi_{bs}; \theta_{bi}, \phi_{bi} = 0) \\ f_{h_b v_b}(\theta_{bs}, \phi_{bs}; \theta_{bi}, \phi_{bi} = 0) & f_{h_b h_b}(\theta_{bs}, \phi_{bs}; \theta_{bi}, \phi_{bi} = 0) \end{bmatrix} \begin{bmatrix} \hat{v}_{bi} \cdot \hat{v}_i & \hat{v}_{bi} \cdot \hat{h}_i \\ \hat{h}_{bi} \cdot \hat{v}_i & \hat{h}_{bi} \cdot \hat{h}_i \end{bmatrix} \tag{53}$$

where

$$\hat{3}_i = \sin\theta_i \cos\phi_i \hat{x} + \sin\theta_i \sin\phi_i \hat{y} + \cos\theta_i \hat{z} \tag{54}$$

$$\hat{v}_i = \cos\theta_i \cos\phi_i \hat{x} + \cos\theta_i \sin\phi_i \hat{y} - \sin\theta_i \hat{z} \tag{55}$$

$$\hat{h}_i = -\sin\phi_i \hat{x} + \cos\phi_i \hat{y} \tag{56}$$

$$\hat{3}_s = \sin\theta_s \cos\phi_s \hat{x} + \sin\theta_s \sin\phi_s \hat{y} + \cos\theta_s \hat{z}$$

$$= \sin\theta_{bs} \cos\phi_{bs} \hat{x}_b + \sin\theta_{bs} \sin\phi_{bs} \hat{y}_b + \cos\theta_{bs} \hat{z}_b \tag{57}$$

$$\hat{v}_s = \cos\theta_s \cos\phi_s \hat{x} + \cos\theta_s \sin\phi_s \hat{y} - \sin\theta_s \hat{z} \tag{58}$$

$$\hat{h}_s = -\sin\phi_s \hat{x} + \cos\phi_s \hat{y} \tag{59}$$

$$\hat{v}_{bs} = \cos\theta_{bs} \cos\phi_{bs} \hat{x}_b + \cos\theta_{bs} \sin\phi_{bs} \hat{y}_b - \sin\theta_{bs} \hat{z}_b \tag{60}$$

$$\hat{h}_{bs} = -\sin\phi_{bs} \hat{x}_b + \cos\phi_{bs} \hat{y}_b \tag{61}$$

$$\hat{y}_b = \frac{\hat{z}_b \times \hat{3}_i}{\sin\theta_{bi}} \tag{62}$$

Note that the angle θ_{bi} can be related to θ_i and ϕ_i by using (28), (30), (32), (54), and (62). It depends on the orientation of the body axis $\hat{z}_b$ as represented by the orientation angles α and β of (28). Similarly, θ_{bs} and ϕ_{bs} can be related to θ_s and ϕ_s by using (28), (57), and (62).

To find the absorption cross section so as to apply (20), (21), and (27) to find the imaginary parts of the forward scattering amplitudes, we first calculate the imaginary parts of the forward scattering amplitudes and the absorption cross sections in the body frame. The absorption cross sections are calculated by assuming that the internal fields of the cylinder are the same as that of the infinite cylinder.

$$\eta \int_{V_b} d\bar{r}' \omega \epsilon''_p \left| \overline{E}^{\gamma_b}_p (\bar{r}') \right|^2$$

$$= 2\pi k L a^4 \frac{\epsilon''_p}{\epsilon} \left\{ \left[\frac{|C_m|^2 k^2_{zbi} + |\eta D_m|^2 k^2}{|w_p|^2 (w_p^2 - w_p^{*2})} \left[w_p J_m(w_p) J'_m(w_p^*) - w_p^* J_m(w_p^*) J'_m(w_p) \right] \right. \right.$$

$$- 2\mathrm{Re} \left[\frac{i k_{zbi} C_m \eta D^*_m k m J_m(w_p) J_m(w_p^*)}{|w_p|^4} \right]$$

$$\left. \left. + \frac{|C_m|^2 \left[w_p^* J_m(w_p) J'_m(w_p^*) - w_p J_m(w_p^*) J'_m(w_p) \right]}{(w_p^2 - w_p^{*2}) a^2} \right] \right\} \tag{63}$$

$$\frac{4\pi}{k} \mathrm{Im} f_{\gamma_b \gamma_b}(\theta_{bi}, \phi_{bi} = 0; \theta_{bi}, \phi_{bi} = 0)$$

$$= \eta \int_{V_p} d\bar{r}' \omega \epsilon''_p \left| \overline{E}^{\gamma_b}_p (\bar{r}') \right|^2$$

$$+ 2\pi \int_0^{\pi} d\theta_{bs} \sin\theta_{bs} a^2 \frac{\sin^2\left(k \frac{L}{2}(\cos\theta_{bs} - \cos\theta_{bi})\right)}{k(\cos\theta_{bs} - \cos\theta_{bi})} \sum_{m=-\infty}^{\infty} \left[\left| F_{v_b m} \right|^2 + \left| F_{h_b m} \right|^2 \right] \tag{64}$$

with $\gamma_b = v_b,\ h_b$. For $\gamma_b = v_b$, we set ($E_{vbi} = 1,\ E_{hbi} = 0$) to calculate the C_m and ηD_m in (35) and (36). For $\gamma_b = h_b$, we set ($E_{vbi} = 0,\ E_{hbi} = 1$) to calculate the C_m and ηD_m in (35) and (36). In the body frame,

$$\mathrm{Im} f_{v_b h_b}(\theta_{bi}, \phi_{bi} = 0; \theta_{bi}, \phi_{bi} = 0) = \mathrm{Im} f_{h_b v_b}(\theta_{bi}, \phi_{bi} = 0; \theta_{bi}, \phi_{bi} = 0) = 0 \tag{65}$$

To find the forward scattering amplitudes in the principal frame, we use (53) and

65) to obtain

$$\text{Im}\, f_{vv}(\theta_i,\phi_i;\theta_i,\phi_i) = \left(\text{Im}\, f_{v_bv_b}(\theta_{bi},\phi_{bi}=0;\theta_{bi},\phi_{bi}=0)\right)(\hat{v}_i\cdot\hat{v}_{bi})^2 + \left(\text{Im}\, f_{h_bh_b}(\theta_{bi},\phi_{bi}=0;\theta_{bi},\phi_{bi}=0)\right)\left(\hat{v}_i\cdot\hat{h}_{bi}\right)^2 \quad (66)$$

$$\text{Im}\, f_{hh}(\theta_i,\phi_i;\theta_i,\phi_i) = \left(\text{Im}\, f_{v_bv_b}(\theta_{bi},\phi_{bi}=0;\theta_{bi},\phi_{bi}=0)\right)\left(\hat{h}_i\cdot\hat{v}_{bi}\right)^2 + \left(\text{Im}\, f_{h_bh_b}(\theta_{bi},\phi_{bi}=0;\theta_{bi},\phi_{bi}=0)\right)\left(\hat{h}_{bi}\cdot\hat{h}_i\right)^2 \quad (67)$$

$$\text{Im}\, f_{vh}(\theta_i,\phi_i;\theta_i,\phi_i) = \left(\text{Im}\, f_{v_bv_b}(\theta_{bi},\phi_{bi}=0;\theta_{bi},\phi_{bi}=0)\right)(\hat{v}_i\cdot\hat{v}_{bi})\left(\hat{h}_i\cdot\hat{v}_{bi}\right) + \left(\text{Im}\, f_{h_bh_b}(\theta_{bi},\phi_{bi}=0;\theta_{bi},\phi_{bi}=0)\right) \times\left(\hat{v}_i\cdot\hat{h}_{bi}\right)\left(\hat{h}_{bi}\cdot\hat{v}_i\right) \quad (68)$$

$$\text{Im}\, f_{hv}(\theta_i,\phi_i;\theta_i,\phi_i) = \left(\text{Im}\, f_{v_bv_b}(\theta_{bi},\phi_{bi}=0;\theta_{bi},\phi_{bi}=0)\right)\left(\hat{h}_i\cdot\hat{v}_{bi}\right)(\hat{v}_i\cdot\hat{v}_{bi}) + \left(\text{Im}\, f_{h_bh_b}(\theta_{bi},\phi_{bi}=0;\theta_{bi},\phi_{bi}=0)\right) \times\left(\hat{h}_{bi}\cdot\hat{h}_i\right)\left(\hat{v}_i\cdot\hat{h}_{bi}\right) \quad (69)$$

Note that the results in this section are calculated for one finite cylinder with orientation in terms of α and β as given by (28). In Section VI, these will be averaged over orientations.

V. METHOD OF MOMENTS AND ENERGY CONSERVATION

We also use a method of moment (MOM) body of revolution code [21,22] to calculate scattering from a finite cylinder. In this code, surface integral equations are solved by using the method of moments. The variations of the unknown electric and magnetic surface fields are approximated by staggered pulse functions in the t-direction and are expanded in Fourier series in the ϕ-direction. The detailed discretization procedure can be found in [21] and [22]. For computational efficiency, it is important to note that it is required to calculate the inverse of the impedance matrix or admittance matrix only once for a cylinder of fixed length, radius, and permittivity. The admittance matrix of the cylinder is then stored. Given incident fields of arbitrary polarization, incident angle, and orientation of the cylinder, the surface fields induced on the surface of the cylinder are calculated by multiplying the admittance matrix with the incident field. In this case, the total surface fields on the curved sides as well as on the two ends of the cylinder are calculated. The bistatic scattering amplitudes can then be calculated. In our implementation, we further store the bistatic scattering amplitudes in the body frame for each harmonic. For an arbitrary incident field and with arbitrary orientation, the bistatic scattering amplitudes in the principal frame can be calculated from that of the stored scattering amplitudes by rotation of coordinates and by interpolation. We also carry out the energy conservation test for the code. The code not only satisfies energy conservation but also reciprocity.

Step 1: Calculation of Impedance Matrix and Admittance Matrix

Given the length, radius, and complex permittivity of the cylinder, the impedance matrix and the admittance matrix of the cylinder are calculated by solving the surface integral equations only one time using the Method of Moment Body of Revolution Code [21,22]. The admittance matrix is then stored.

Step 2: Calculation of Bistatic Scattering Amplitudes for Each Harmonic in the Body Frame

Consider an incident field given in the body frame by

$$\overline{E}^i = \left(E_{vbi}\,\hat{v}_{bi} + E_{hbi}\,\hat{h}_{bi}\right) \quad (70)$$

$$\hat{s}_i = \sin\theta_{bi}\,\hat{x}_b + \cos\theta_{bi}\,\hat{z}_b \quad (71)$$

$$\hat{v}_{vi} = \cos\theta_{bi}\,\hat{x}_b - \sin\theta_{bi}\,\hat{z}_b \quad (72)$$

$$\hat{h}_{bi} = \hat{y}_b \quad (73)$$

Because of rotational symmetry, we have taken $\phi_{bi}=0$ without loss of generality. Given the admittance matrix stored in step 1, a product can be taken between the admittance matrix and the incident field to give the surface fields at each discretized point on the surface for each harmonic. These include $E^C_{\phi m}(z_b)$, $H^C_{\phi m}(z_b)$, $E^C_{zm}(z_b)$, and $H^C_{zm}(z_b)$ on the curved side, $E^U_{\rho m}(\rho_b)$, $H^U_{\rho m}(\rho_b)$, $E^U_{\phi m}(\rho_b)$, and $H^U_{\phi m}(\rho_b)$ on the upper side, and $E^L_{\rho m}(\rho_b)$, $H^L_{\rho m}(\rho_b)$, $E^L_{\phi m}(\rho_b)$, and $H^L_{\phi m}(\rho_b)$ on the lower side, where z_b denotes the coordinate on the curved side and ρ_b denotes the cylindrical radial coordinate on the upper side and the lower side. The bistatic scattering amplitudes in the body frame are

$$f_{v_bv_b}(\theta_{bs},\phi_{bs};\theta_{bi},\phi_{bi}=0) = \sum_{m=-\infty}^{\infty} e^{im\phi_{bs}}\, f_{v_bv_bm}(\theta_{bs},\theta_{bi}) \quad (74)$$

$$f_{v_bh_b}(\theta_{bs},\phi_{bs};\theta_{bi},\phi_{bi}=0) = \sum_{m=-\infty}^{\infty} e^{im\phi_{bs}}\, f_{v_bh_bm}(\theta_{bs},\theta_{bi}) \quad (75)$$

$$f_{h_bv_b}(\theta_{bs},\phi_{bs};\theta_{bi},\phi_{bi}=0) = \sum_{m=-\infty}^{\infty} e^{im\phi_{bs}}\, f_{h_bv_bm}(\theta_{bs},\theta_{bi}) \quad (76)$$

$$f_{h_bh_b}(\theta_{bs},\phi_{bs};\theta_{bi},\phi_{bi}=0) = \sum_{m=-\infty}^{\infty} e^{im\phi_{bs}}\, f_{h_bh_bm}(\theta_{bs},\theta_{bi}) \quad (77)$$

The bistatic scattering amplitudes for each harmonic, $f_{v_bv_bm}(\theta_{bs},\theta_{bi})$, $f_{v_bh_bm}(\theta_{bs},\theta_{bi})$, $f_{h_bv_bm}(\theta_{bs},\theta_{bi})$, and $f_{h_bh_bm}(\theta_{bs},\theta_{bi})$ can be expressed in terms of the surface fields as follows

$$f_{v_b\delta_bm}(\theta_{bs},\theta_{bi}) = (-i)^m\,\frac{a}{2}\Big[-ik\left\{\sin\theta_{bs}\eta H_{\phi m}J_m(w_s) + \frac{m}{w_s}\cos\theta_{bs}\eta H_{zm}J_m(w_s)\right\} - kE_{zm}J'_m(w_s)\Big]$$

$$+\frac{(-i)^m}{2}e^{ik(\cos\theta_{bi}-\cos\theta_{bs})\frac{L}{2}}\int_0^a d\rho_b\rho_b\left[\frac{imk}{k\sin\theta_{bs}\rho_b}J_m(k\sin\theta_{bs}\rho_b)\right.$$
$$\times\left\{-E^U_{\phi m}(\rho_b)+\eta H^U_{\rho m}(\rho_b)\cos\theta_{bs}\right\}$$
$$\left.+kJ'_m(k\sin\theta_{bs}\rho_b)\left\{E^U_{\rho m}(\rho_b)+\eta H^U_{\phi m}(\rho_b)\cos\theta_{bs}\right\}\right]$$
$$+\frac{(-i)^m}{2}e^{-ik(\cos\theta_{bi}-\cos\theta_{bs})\frac{L}{2}}\int_0^a d\rho_b\rho_b\left[-\frac{imk}{k\sin\theta_{bs}\rho_b}J_m(k\sin\theta_{bs}\rho_b)\right.$$
$$\times\left\{-E^L_{\phi m}(\rho_b)+\eta H^L_{\rho m}(\rho_b)\cos\theta_{bs}\right\}$$
$$\left.-kJ'_m(k\sin\theta_{bs}\rho_b)\left\{E^L_{\rho m}(\rho_b)+\eta H^L_{\phi m}(\rho_b)\cos\theta_{bs}\right\}\right] \quad (78)$$

$$f_{h_b\delta_b m}(\theta_{bs},\theta_{bi})=(-i)^m\frac{a}{2}\left[-ik\left\{\sin\theta_{bs}E_{\phi m}J_m(w_s)\right.\right.$$
$$\left.+\frac{m}{w_s}\cos\theta_{bs}E_{zm}J_m(w_s)\right\}+k\eta H_{zm}J'_m(w_s)\Big]$$
$$+\frac{(-i)^m}{2}e^{ik(\cos\theta_{bi}-\cos\theta_{bs})\frac{L}{2}}\int_0^a d\rho_b\rho_b\left[\frac{imk}{k\sin\theta_{bs}\rho_b}J_m(k\sin\theta_{bs}\rho_b)\right.$$
$$\times\left\{\eta H^U_{\phi m}(\rho_b)+E^U_{\rho m}(\rho_b)\cos\theta_{bs}\right\}$$
$$\left.+kJ'_m(k\sin\theta_{bs}\rho_b)\left\{-\eta H^U_{\rho m}(\rho_b)+E^U_{\phi m}(\rho_b)\cos\theta_{bs}\right\}\right]$$
$$+\frac{(-i)^m}{2}e^{-ik(\cos\theta_{bi}-\cos\theta_{bs})\frac{L}{2}}\int_0^a d\rho_b\rho_b\left[-\frac{imk}{k\sin\theta_{bs}\rho_b}J_m(k\sin\theta_{bs}\rho_b)\right.$$
$$\times\left\{E^L_{\rho m}(\rho_b)\cos\theta_{bs}+\eta H^L_{\phi m}(\rho_b)\right\}$$
$$\left.-kJ'_m(k\sin\theta_{bs}\rho_b)\left\{E^L_{\phi m}(\rho_b)\cos\theta_{bs}-\eta H^L_{\rho m}(\rho_b)\right\}\right] \quad (79)$$

where $\delta=v,h$

$$w_s=k\sin\theta_{bs} \quad (80)$$

$$H_{\phi m}=\int_{-\frac{L}{2}}^{\frac{L}{2}}dz_b\,e^{ik(\cos\theta_{bi}-\cos\theta_{bs})z_b}H^C_{\phi m}(z_b) \quad (81)$$

$$H_{zm}=\int_{-\frac{L}{2}}^{\frac{L}{2}}dz_b\,e^{ik(\cos\theta_{bi}-\cos\theta_{bs})z_b}H^C_{zm}(z_b) \quad (82)$$

$$E_{\phi m}=\int_{-\frac{L}{2}}^{\frac{L}{2}}dz_b\,e^{ik(\cos\theta_{bi}-\cos\theta_{bs})z_b}E^C_{\phi m}(z_b) \quad (83)$$

$$E_{zm}=\int_{-\frac{L}{2}}^{\frac{L}{2}}dz_b\,e^{ik(\cos\theta_{bi}-\cos\theta_{bs})z_b}E^C_{zm}(z_b) \quad (84)$$

For $\delta_b=v_b$, we set $(E_{vbi}=1,\ E_{hbi}=0)$ to calculate the surface fields from the admittance matrix. For $\delta_b=h_b$, we set $(E_{vbi}=0,\ E_{hbi}=1)$ to calculate the surface fields from the admittance matrix. The bistatic scattering amplitudes for each harmonic $f_{v_bv_bm}(\theta_{bs},\theta_{bi})$, $f_{v_bh_bm}(\theta_{bs},\theta_{bi})$, $f_{h_bv_bm}(\theta_{bs},\theta_{bi})$, and $f_{h_bh_bm}(\theta_{bs},\theta_{bi})$ can be stored for a two dimensional array of values of θ_{bs} and θ_{bi}. The bistatic scattering amplitudes for each harmonic at arbitrary values of θ_{bs} and θ_{bi} can then be calculated by interpolation.

Step 3: Calculation of Bistatic Scattering Amplitude in the Principal Frame

For an incident plane wave in the direction $\hat{s}_i$ as given by (54) impinging upon the cylinder with body axis

$$\hat{z}_b=\sin\beta\cos\alpha\,\hat{x}+\sin\beta\sin\alpha\,\hat{y}+\cos\beta\,\hat{z} \quad (28)$$

the transformation of bistatic scattering amplitudes between the principal frame and the body frame follows that of (53)–(62). Calculation of body frame scattering amplitudes are done by using (74)–(77) and interpolation.

We also carry out energy conservation tests. For the case of real permittivity ϵ_p without absorption loss, the optical theorem can be verified by checking the equality of extinction and scattering cross sections. Thus for the case of real ϵ_p, the following relations from (20) to (21) have to be obeyed to satisfy energy conservation.

$$\frac{4\pi}{k}\,\mathrm{Im}\,f_{\delta_b\delta_b}(\theta_{bi},\phi_{bi}=0;\theta_{bi},\phi_{bi}=0)$$
$$=2\pi\int_0^\pi d\theta_{bs}\sin\theta_{bs}\sum_{m=-\infty}^{\infty}\left[\left|f_{v_b\delta_bm}(\theta_{bs},\theta_{bi})\right|^2+\left|f_{h_b\delta_bm}(\theta_{bs},\theta_{bi})\right|^2\right] \quad (85)$$

for $\delta_b=v_b,h_b$. In our calculations, we have checked energy conservation for the method of moment code by using (85).

VI. NUMERICAL RESULTS AND DISCUSSIONS

In this section, we illustrate the numerical results of radar polarimetry of a layer of dielectric cylinders overlying a homogeneous half space using parameters of vegetation and soil [23–25]. The special case of statistical azimuthal symmetry will be examined. Thus for a function that depends on the orientation angles α and β, the averaging of the function $g(\alpha,\beta)$ is taken as follows

$$<g(\alpha,\beta)>=\frac{1}{\cos\beta_1-\cos\beta_2}\int_{\beta_1}^{\beta_2}d\beta\sin\beta\int_0^{2\pi}d\alpha\,g(\alpha,\beta) \quad (86)$$

The probability density function is uniform for solid angles with α between 0 and 2π, and β between β_1 and β_2. The $\sin\beta$ factor in (86) accounts for the differential solid angle. The results of copolarized return, depolarized return, degree of polarization, and the phase differences [28] are illustrated for first order and second order solution. The first order solution consists of the sum of the first four terms in (16) (i.e., a, b, c, and d). The second order solution refers to the sum of all five terms in (16) (a, b, c, d, e). In all the figures we only show the results of MOM combined with the vector radiative transfer theory. The corresponding Mueller matrices are tabulated. Some of the Mueller matrices based on the infinite

cylinder approximation are also listed in the tables for comparison.

In Fig. 3, we plot the copolarized return, depolarized return, and degree of polarization for a medium of cylinders of length 15 cm and radius 2.5 cm at L band based on first order theory and MOM. The Mueller matrices of MOM, the infinite cylinder approach with scattered field and that with total field, are all listed in Table I for comparison. The absorption coefficients, scattering coefficients, and extinction coefficients for V and H polarizations are all listed so that the optical thicknesses can be calculated readily to see whether higher order scattering effects are important. We note from the tabulated Mueller matrices that there is some difference between the scattered field approximation and the total field approximation. However, there are large differences with the MOM results. This is because for this case, the radius of the cylinder is not small and significant errors are in the infinite cylinder approximation because the scattering-induced radiation from the ends of the cylinders are neglected. Also results based on the infinite cylinder approach do not obey reciprocity. That is, VH is not equal to HV. Some of the terms in the first order solution include scattering by the cylinder as well as reflection by the boundary. For example, the term that corresponds to first scattering by the cylinder and then reflection by the boundary makes use of the bistatic scattering amplitude of the cylinder which is not reciprocal in the infinite cylinder approximation. On the other hand, the MOM solution is reciprocal. The cylinders are uniformly oriented for β between 0° and 45°. As indicated in Fig. 3a, the HH return is larger than the VV return because of the randomness of orientation and the large radius of the cylinder. The results in Fig. 3 also indicate large variation of scattering with polarization.

0.549E-02	0.188E-02	0.000	0.000
0.167E-02	0.593E-02	0.000	0.000
0.000	0.000	-0.481E-03	0.798E-03
0.000	0.000	-0.829E-03	0.354E-03

(1) Infinite cylinder scattered field approximation

(The computed values of absorption and scattering rates based on infinite cylinder scattered field approximations are $\kappa_{av} = 0.138\,\mathrm{m}^{-1}$, $\kappa_{sv} = 0.201\,\mathrm{m}^{-1}$, $\kappa_{ah} = 0.0872\,\mathrm{m}^{-1}$, $\kappa_{sh} = 0.0926\,\mathrm{m}^{-1}$).

0.552E-02	0.189E-02	0.000	0.000
0.169E-02	0.604E-02	0.000	0.000
0.000	0.000	-0.575E-03	0.998E-03
0.000	0.000	-0.961E-03	0.227E-03

(2) Infinite Cylinder total field approximation

0.882E-02	0.168E-02	0.000	0.000
0.168E-02	0.101E-01	0.000	0.000
0.000	0.000	-.277E-02	0.184E-02
0.000	0.000	-.184E-02	-.939E-03

(3) Method of Moment solution

(The computed values of extinction rates are $\kappa_{ev} = 0.4037\,\mathrm{m}^{-1}$, $\kappa_{eh} = 0.2324\,\mathrm{m}^{-1}$).

Table I. Mueller matrices of Fig. 3.

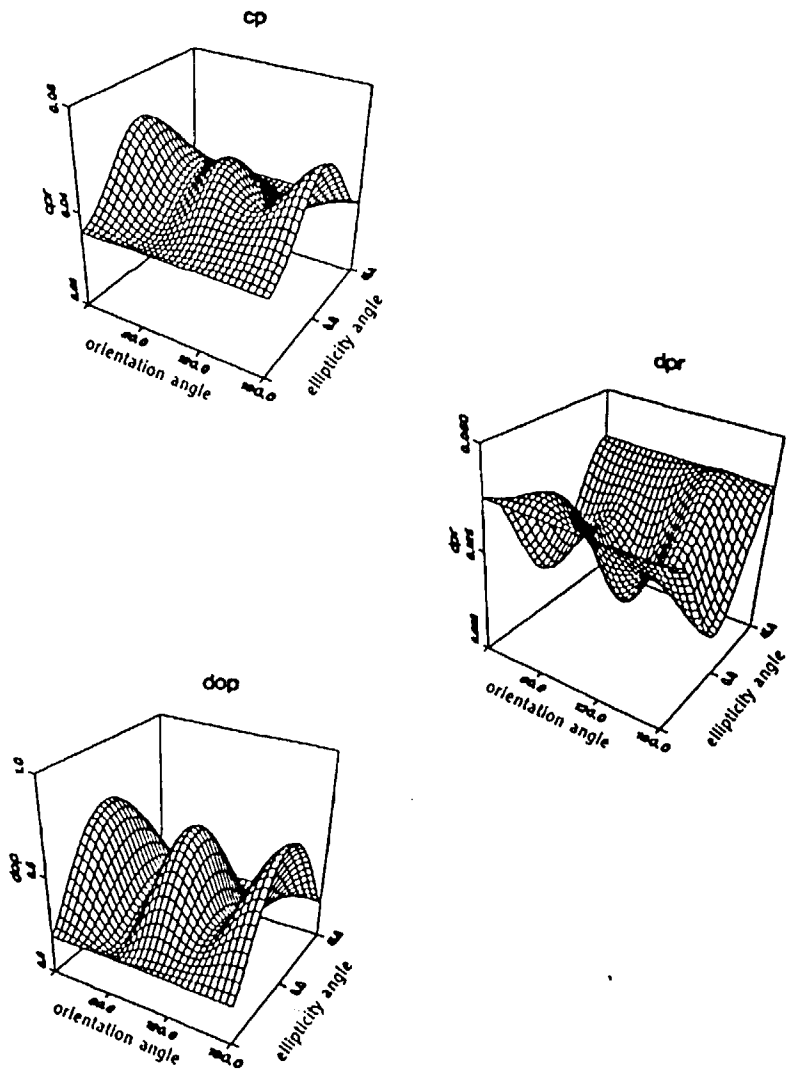

Figure 3. Polarimetric signatures based on first order theory and MOM code as a function of ellipticity angle χ and orientation angle Ψ of a layer of dielectric cylinders with prescribed orientation distribution (a) copolarized return, (b) depolarized return, and (c) degree of polarization. The parameters are: frequency = 1.225 GHz, $\epsilon_s = (6.5+i2)\epsilon_0$, $a = 2.5$ cm, $L = 15$ cm, fractional volume=0.006, $d = 0.5$ meters, $\epsilon_2 = (15+i2)\epsilon_0$, and $\theta_0 = \theta_s = 60°$. Orientation distribution is governed by $\beta_1 = 0°$ and $\beta_2 = 45°$. The values of the Mueller matrices based on MOM and infinite cylinder approximations are listed in Table I.

In Fig. 4, we show the case for cylinders with a smaller radius of $a = 1$ cm. The corresponding Mueller matrices for the three approaches are shown in Table II. Because of the smaller radius compared with wavelength, the results of the infinite cylinder approximation are in good agreement with MOM. The copolarized return indicate that VV is larger than HH for this case of slender cylinders. The copolarized return and the depolarized return also show that the variations of scattering with polarization are less rapid than that of Fig. 3.

In Figs. 5 and 6, we show respectively the results of first order theory and second order theory using the same parameters of Fig. 3 but with a larger layer thickness of $d = 2.5$ meters. The Mueller matrices are listed in Table III. The optical thicknesses are 1.01 and 0.58 respectively for vertical and horizontal polarizations. There is a significant amount of multiple scattering in this case as seen by the differences in results between the two figures. The Mueller matrices are listed in Table III. Inclusion of second order scattering significantly increases the contrast between the VV and HH return. It also significantly increases the depolarized return. The results also indicate that multiple scattering can be important at L band for some cases of medium parameters.

0.740E-02	0.126E-02	0.000	0.000
0.128E-02	0.411E-02	0.000	0.000
0.000	0.000	-0.181E-02	0.589E-03
0.000	0.000	-0.591E-03	-0.104E-02

(1) Infinite cylinder scattered field approximation

(The computed values of absorption and scattering rates based on infinite cylinder scattered field approximations are $\kappa_{av} = 0.245\,\mathrm{m}^{-1}$ $\kappa_{sv} = 0.118\,\mathrm{m}^{-1}$ $\kappa_{ah} = 0.0764\,\mathrm{m}^{-1}$ $\kappa_{sh} = 0.0318\,\mathrm{m}^{-1}$).

0.741E-02	0.128E-02	0.000	0.000
0.127E-02	0.411E-02	0.000	0.000
0.000	0.000	-0.183E-02	0.586E-03
0.000	0.000	-0.572E-03	-0.107E-02

(2) Infinite Cylinder total field approximation

0.703E-02	0.987E-03	0.000	0.000
0.987E-03	0.446E-02	0.000	0.000
0.000	0.000	-.204E-02	0.485E-03
0.000	0.000	-.485E-03	-.134E-02

(3) Method of Moments solution

(The computed values of extinction rates are $\kappa_{ev} = 0.2955\,\mathrm{m}^{-1}$ $\kappa_{eh} = 0.0953\,\mathrm{m}^{-1}$).

Table II. Mueller matrices of Fig. 4

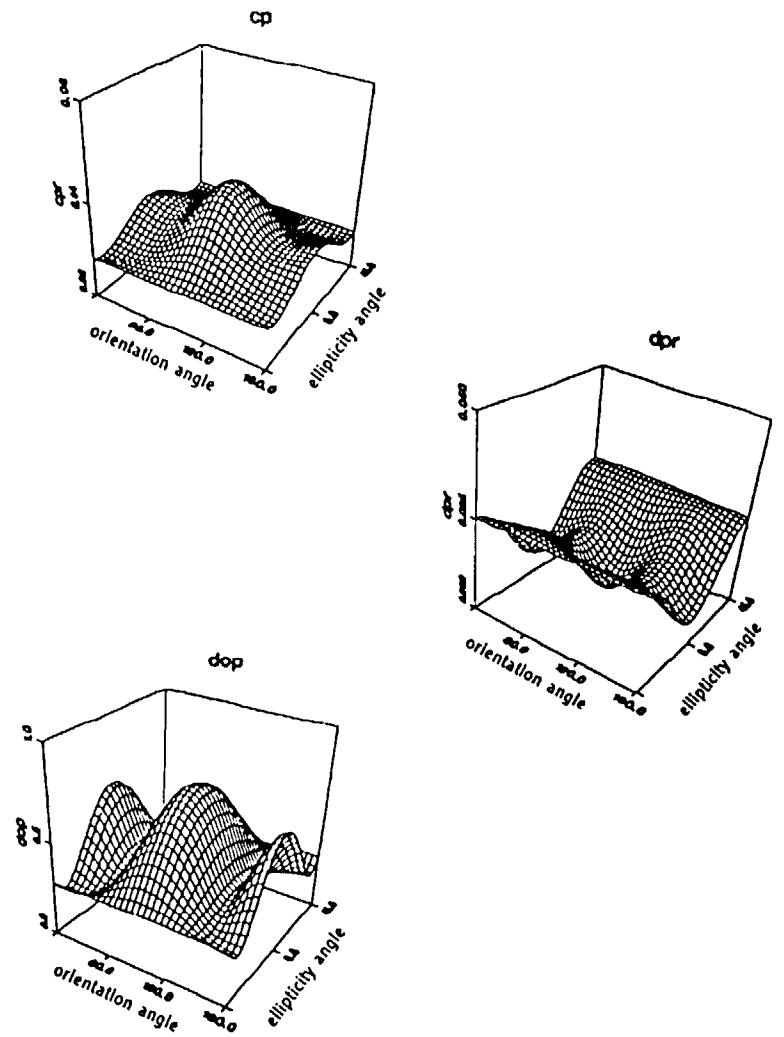

Figure 4. Polarimetric signatures based on first order theory and MOM code as a function of ellipticity angle χ and orientation angle Ψ of a layer of dielectric cylinders with prescribed orientation distribution (a) copolarized return, (b) depolarized return, and (c) degree of polarization. The parameters are: frequency = 1.225 GHz, $\varepsilon_s = (6.5 + i2)\varepsilon_0$, $a = 1$ cm, $L = 15$ cm., fractional volume=0.006, $d = 0.5$ meters, $\varepsilon_2 = (15 + i2)\varepsilon_0$, and $\theta_0 = \theta_s = 60°$. Orientation distribution is governed by $\beta_1 = 0°$ and $\beta_2 = 45°$. The values of the Mueller matrices based on MOM and infinite cylinder approximations are listed in Table II.

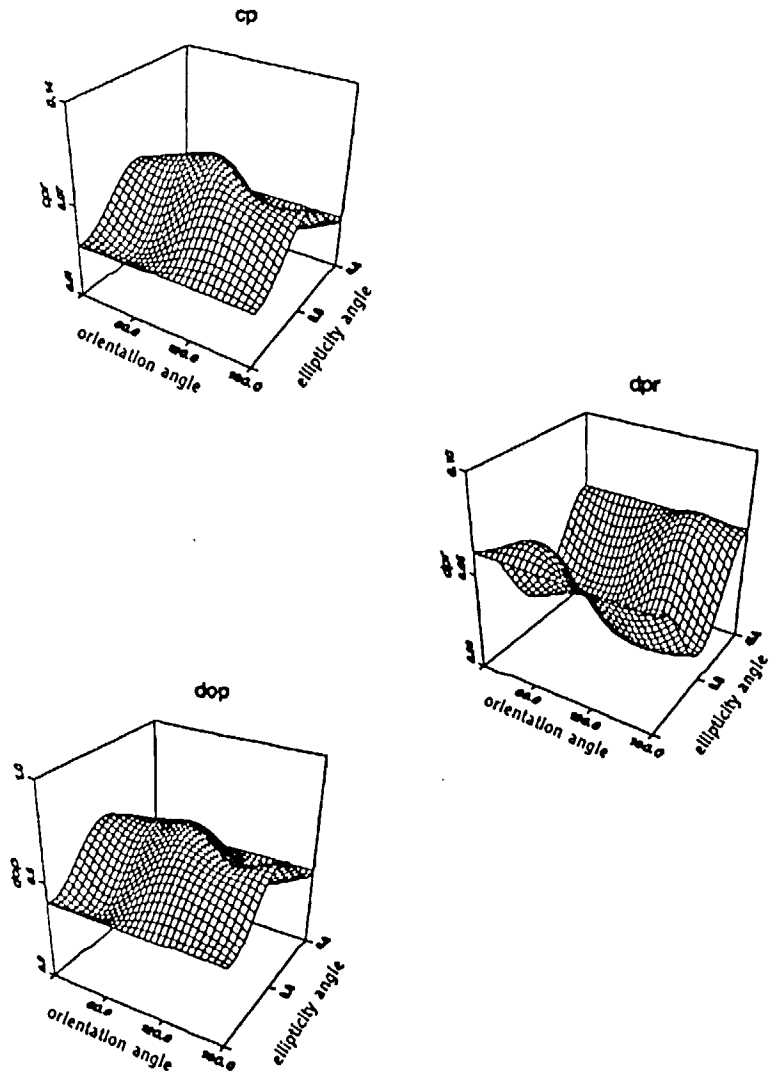

Figure 5. Polarimetric signatures based on first order theory and MOM code as a function of ellipticity angle χ and orientation angle Ψ of a layer of dielectric cylinders with prescribed orientation distribution (a) copolarized return, (b) depolarized return, and (c) degree of polarization. The parameters are: frequency = 1.225 GHz, $\epsilon_s = (6.5+i2)\epsilon_0$, $a = 2.5$ cm, $L = 15$ cm, fractional volume=0.006, $d = 2.5$ meters, $\epsilon_2 = (15 + i2)\epsilon_0$, and $\theta_0 = \theta_s = 60°$. Orientation distribution is governed by $\beta_1 = 0°$ and $\beta_2 = 45°$. The values of the Mueller matrices based on MOM are listed in Table III.

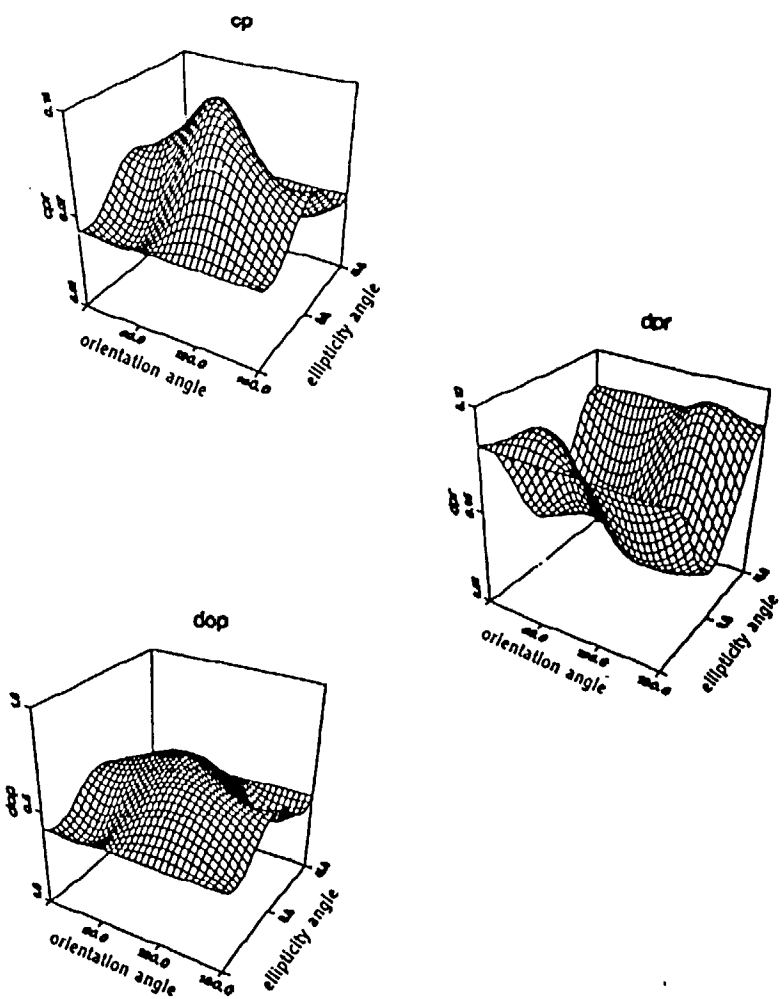

Figure 6. Polarimetric signatures based on second order theory and MOM code as a function of ellipticity angle χ and orientation angle Ψ of a layer of dielectric cylinders with prescribed orientation distribution (a) copolarized return, (b) depolarized return, and (c) degree of polarization. The parameters are: frequency = 1.225 GHz, $\epsilon_s = (6.5+i2)\epsilon_0$, $a = 2.5$ cm, $L = 15$ cm, fractional volume=0.006, $d = 2.5$ meters, $\epsilon_2 = (15 + i2)\epsilon_0$, and $\theta_0 = \theta_s = 60°$. Orientation distribution is governed by $\beta_1 = 0°$ and $\beta_2 = 45°$. The values of the Mueller matrices based on MOM are listed in Table III.

0.149E-01	0.263E-02	0.000	0.000
0.263E-02	0.122E-01	0.000	0.000
0.000	0.000	-.788E-02	0.537E-02
0.000	0.000	-.537E-02	-.335E-02

Mueller matrices of Fig. 5 (first order solution)

0.219E-01	0.421E-02	0.000	0.000
0.422E-02	0.143E-01	0.000	0.000
0.000	0.000	-.101E-01	0.735E-02
0.000	0.000	-.737E-02	-.367E-02

Mueller matrix of Fig. 6 (second order solution)

Table III. (The computed values of extinction rates are $\kappa_{ev} = 0.4037\,\mathrm{m}^{-1}$ $\kappa_{eh} = 0.2324\,\mathrm{m}^{-1}$).

In Figs. 7 and 8, the results at C band for the first order solution and second order solution are shown respectively. The Mueller matrices are listed in Table IV. The second order solution show a stronger contrast between VV and HH returns. It also shows larger depolarization return than the first order solution. There is strong depolarization even for linearly polarized waves. The results indicate that multiple scattering effects are generally important at C band.

0.296E-01	0.156E-02	0.000	0.000
0.156E-02	0.288E-01	0.000	0.000
0.000	0.000	-.166E-01	0.122E-01
0.000	0.000	-.122E-01	-.141E-01

Mueller matrices of Fig. 7 (first order solution)

0.436E-01	0.316E-02	0.000	0.000
0.316E-02	0.327E-01	0.000	0.000
0.000	0.000	-.193E-01	0.164E-01
0.000	0.000	-.164E-01	-.146E-01

Mueller matrix of Fig. 8 (Second order solution)

Table IV. (The computed values of extinction rates are $\kappa_{ev} = 0.2353\,\mathrm{m}^{-1}$ $\kappa_{eh} = 0.1068\,\mathrm{m}^{-1}$).

In Fig. 9, we plot the phase difference (i.e., phase at which the probability density function is maximum [28]) as a function of orientation with $\beta_1 = 0$ and β_2 varying between 0 degrees and 90 degrees using the parameters of C band of Figs. 7 and 8. The case of β_2 equal to zero corresponds to vertically aligned cylinders while β_2 equal to 90 degrees corresponds to completely random orientations. As can be seen from the figure, the case of a completely random orientation gives zero phase difference. We also note that the first order theory underestimates the phase difference. The phase difference is positive for cylinders while previous results indicate the phase difference is negative for oblate spheroids [11].

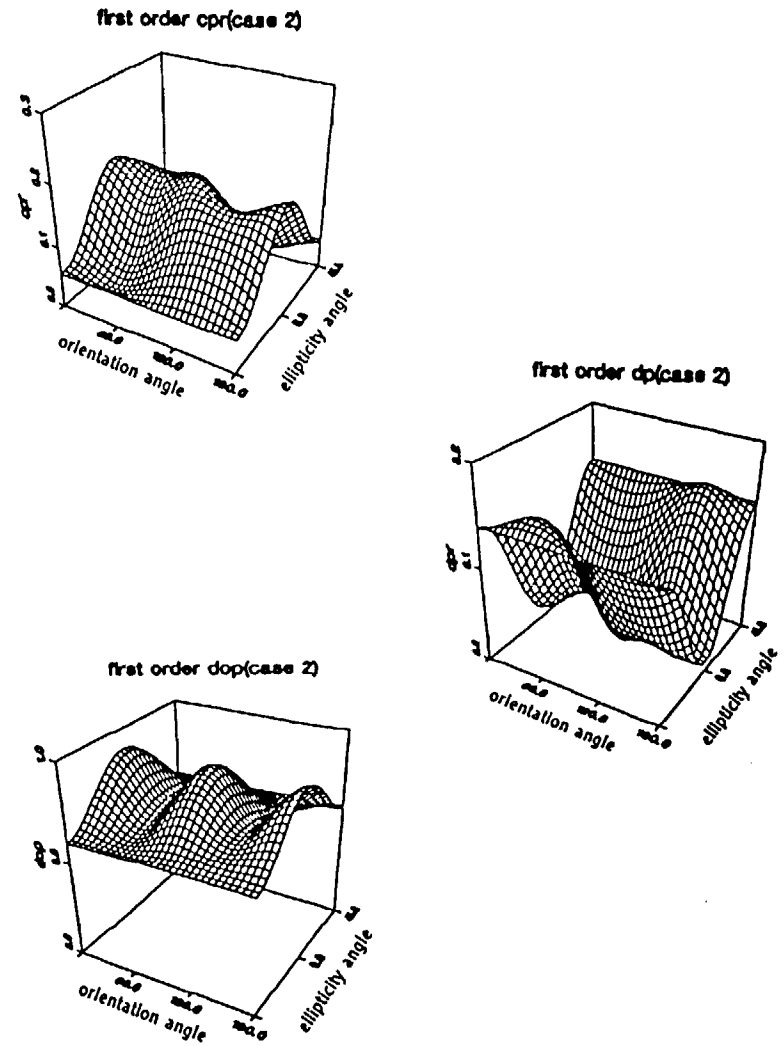

Figure 7. Polarimetric signatures based on first order theory and MOM code as a function of ellipticity angle χ and orientation angle Ψ of a layer of dielectric cylinders with prescribed orientation distribution (a) copolarized return, (b) depolarized return, and (c) degree of polarization. The parameters are: frequency = 5.64 GHz, $\epsilon_s = (3 + i0.06)\epsilon_0$, $a = 0.35\,\mathrm{cm}$, $L = 5\,\mathrm{cm}$, fractional volume=0.006, $d = 2.5$ meters, $\epsilon_2 = (4 + i)\epsilon_0$, and $\theta_0 = \theta_s = 60°$. Orientation distribution is governed by $\beta_1 = 0°$ and $\beta_2 = 45°$. The values of the Mueller matrices based on MOM are listed in Table IV.

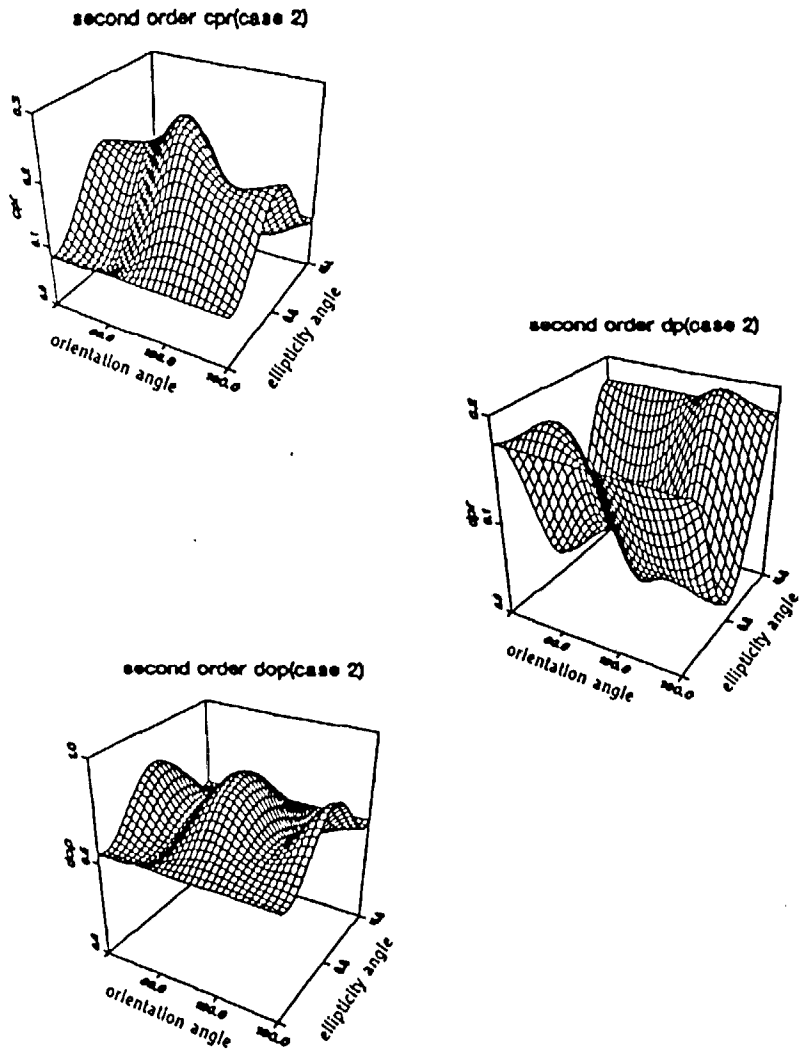

Figure 8. Polarimetric signatures based on second order theory and MOM code as a function of ellipticity angle χ and orientation angle Ψ of a layer of dielectric cylinders with prescribed orientation distribution (a) copolarized return, (b) depolarized return, and (c) degree of polarization. The parameters are: frequency = 5.64 GHz, $\epsilon_s = (3+i0.06)\epsilon_0$, $a = 0.35$ cm, $L = 5$ cm, fractional volume=0.006, $d = 2.5$ meters, $\epsilon_2 = (4+i)\epsilon_0$, $\theta_0 = \theta_s = 60°$. Orientation distribution is governed by $\beta_1 = 0°$ and $\beta_2 = 45°$. The values of the Mueller matrices based on MOM are listed in Table IV.

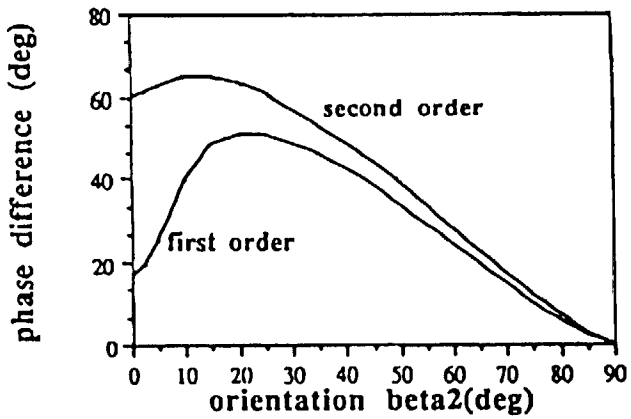

Figure 9. Phase differences (9) based on first order theory and second order theory are compared as a function of orientation distribution. Orientation distribution is governed by $\beta_1 = 0°$ and β_2 varying between 0 degrees and 90 degrees. Phase matrices and extinction matrices are based on MOM code. The parameters are: frequency = 5.64 GHz, $\epsilon_s = (3+i0.06)\epsilon_0$, $a = 0.35$ cm, $L = 5$ cm, fractional volume=0.006, $d = 2.5$ meters, $\epsilon_2 = (4+i)\epsilon_0$, $\theta_0 = \theta_s = 60°$.

In Fig. 10 we make a comparison of total surface fields for $m = 0$ harmonic, computed based on infinite cylinder approximation (IC) and MOM solution using the parameters of the dielectric cylinder of Fig. 3. The incident wave is of unit amplitude in a direction perpendicular to the axis of the cylinder with polarization parallel to the axis of the cylinder. Equivalent electric surface currents ηJ_t and equivalent magnetic surface current M_φ are shown. The t coordinate and the t direction is as indicated in the figure. As shown in Fig. 10, the infinite cylinder approximation has a magnitude of equivalent surface currents uniform along the length of the cylinder while the MOM solution has currents tapering off towards the two endfaces.

In Table V, we compare the CPU time of the various methods that are used in computing the results of Fig. 3. We note that the CPU required for MOM for one cylinder far exceeds that of infinite cylinder approximation. In vector radiative transfer first and second order solutions, however, most of the CPU goes to the computation of averaging over orientations and summing over scattered directions from one cylinder to another. Thus the CPU of MOM becomes a small fraction of the total CPU. As indicated in the table, the total required CPU for the first order solution differs only by a factor of 4 between that of MOM and infinite cylinder approximation.

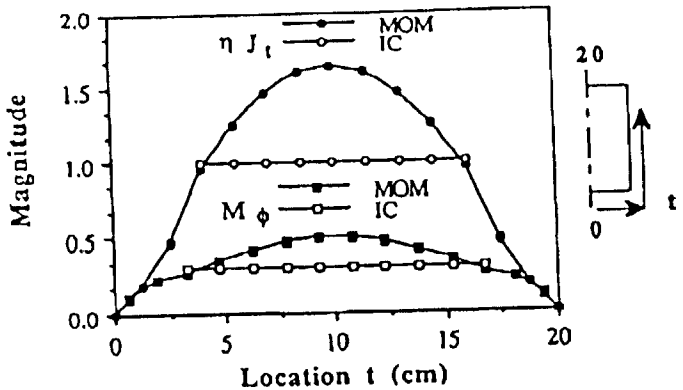

Figure 10. Comparison of total surface fields for $m = 0$ harmonic computed based on infinite cylinder approximation (IC) and MOM solution using parameters of dielectric cyliner of Fig. 3 with frequency = 1.225 GHz, $\epsilon_s = (6.5 + i2)\epsilon_0$, $a = 2.5$ cm, $L = 15$ cm. The incident wave is of unit amplitude in a direction perpendicular to the axis of the cylinder with polarization parallel to the axis of the cylinder. Equivalent electric surface currents ηJ_t and equivalent magnetic surface current M_ϕ are shown. The t coordinate and the t direction is as indicated in the figure. The t coordinate starts from center of bottom face, radially outward to the edge, along the curved side and then ends at the center of the top face with range 2.5 cm + 15 cm + 2.5 cm = 20 cm.

Method	Single Particle Scattering	Vector Radiative Transfer Solution	Total CPU Required
first order vector radiative transfer and MOM	89 sec	391 sec	480 sec
second order vector radiative transfer and MOM	89 sec	5932 sec	6021 sec
first order vector radiative transfer and infinite cylinder approximation			122 sec

Table V. Comparison of CPU of various methods on DEC Station 3100 for computer results of Fig. 3.

ACKNOWLEDGMENTS

The research in this paper was supported by the Army Research Office, NASA, and the National Science Foundation.

The Editor thanks S. S. Seker and two anonymous Reviewers for reviewing the paper.

REFERENCES

1. Huynen, J. R., "Phenomenological theory of radar targets" *Electromagnetic Scattering*, ed. by P. L. E. Uslenghi, 653–712, Academic Press, New York, 1978.
2. Tsang, L., J. A. Kong, and R. T. Shin, *Theory of Microwave Remote Sensing*, Wiley Interscience, New York, 1985.
3. Giuli, D., "Polarization diversity in radars," *Proc. IEEE*, Vol. 74, 245–269, 1986.
4. Ulaby, F. T., and C. Elachi (eds.), *Radar Polarimetry for Geoscience Applications*, Artech. House, Norwood, MA, 1990.
5. Kong, J. A., (ed.), "Polarimetric remote sensing," *Progress in Electromagnetic Research*, Vol. 3, Elsevier, New York, 1990.
6. van Zyl, J. J., H. A. Zebker, and C. Elachi, "Imaging radar polarization signatures: theory and observation," *Radio Science*, Vol. 22, 529–543, 1987.
7. Ulaby, F. T., D. N. Held, M. C. Dobson, K. C. McDonald, and T. B. A. Senior, "Relating polarization difference of SAR signals to scene properties," *IEEE Trans. Geoscience and Remote Sensing*, GE-25, 83–92, 1987.
8. Evans, D. L., T. G. Farr, J. J. van Zyl, and H. A. Zebker, "Radar polarimetry: analysis tools and applications," *IEEE Trans. Geoscience and Remote Sensing*, GE-26, 774–789, 1988.
9. Borgeaud, M., R. T. Shin, and J. A. Kong, "Theoretical models for polarimetric radar clutter," *J. Electromagnetic Waves and Applications*, Vol. 1, 73–89, 1987.
10. Boerner, W. M., B. Y. Foo, and H. J. Eom, "Interpretation of polarimetric copolarization phase term in radar images obtained with the JPL airborne L-band SAR system," *IEEE Trans. Geoscience and Remote Sensing*, GE-25, 77–82, 1987.
11. Tsang, L., K. H. Ding, and B. Wen, "Polarimetric signatures of random discrete scatterers based on vector radiative transfer theory, Part I: Nonspherical particles, and Part II: Dense Media," Chapter 2 of *Polarimetric Remote Sensing*, 75–142, Vol. 3 of *Progress in Electromagnetic Research*, ed. by J. Kong, Elsevier, New York, 1990.
12. Wen, B., L. Tsang, D. P. Winebrenner, and A. Ishimaru, "Dense medium radiative transfer theory: comparison with experiment and application to microwave remote sensing and polarimetry," *IEEE Trans. Geosci. Remote Sensing*, GE-28, 46–59, 1990.
13. Ulaby, F. T., K. Sarabandi, K. McDonald, M. Whitt, and M. C. Dobson, "Michigan microwave canopy scattering model (MIMICS)," *Radiation Laboratory Report 022486-T-1*, Department of Electrical Engineering and Computer Science, The University of Michigan, Ann Arbor, Michigan, July 1988.
14. Chen, Z., M.Sc. Thesis, Department of Electrical Engineering, University of Washington, Seattle, WA 981995, Nov. 1990.
15. Tsang, L., and K. H. Ding, "Polarimetric signatures of a layer of random nonspherical discrete scatterers overlying a homogeneous half space based on first and second order vector radiative transfer theory," *IEEE Trans. on Geoscience and Remote Sensing*, Vol. 29, No. 2, 242–252, March 1991.
16. Chauhan, N. S., and R. H. Lang, "Microwave modelling of orchard canopy," *Proceedings of IGARSS'88*, 1757, Edinburgh, Scotland, 1988.
17. Seker, S. S., and A. Schneider, "Electromagnetic scattering from a dielectric cylinder of finite length," *IEEE Trans. on Antennas and Propagation*, AP-36, 303–307, 1988.
18. Karam, M., and A. K. Fung, "Electromagnetic scattering from a layer of finite length, randomly oriented dielectric circular cylinders over a rough interface with application to vegetation," *Int. J. Remote Sensing*, Vol. 9, 1109–1134, 1988.
19. Born, M., and E. Wolf, *Principles of Optics*, Fifth Editon, Pergamon Press, New York.

20. Karam, M. A., and A. K. Fung, "Vector forward scattering theorem," *Radio Science*, Vol. 17, 752–756, 1982.
21. Glisson, A. W., and D. R. Wilton, "Simple and efficient numerical techniques for treating bodies of revolution," *Technical Report 105*, Engineering Experiment Station, The University of Mississippi, University, Mississippi, March 1979.
22. Joseph, J., "Application of integral equation and finite difference method to electromagnetic scattering by two dimensional and body of revolution geometries," Ph.D. thesis, Department of Electrical and Computer Engineering, University of Illinois at Urbana-Champaign, Urbana, Illinois, May 1990.
23. EL-Rayes, M. A., and F. T. Ulaby, "Microwave dielectric spectrum of vegetation, Part I: Experimental observations," *IEEE Trans. Geoscience and Remote Sensing*, GE-25, 541–549, 1987.
24. Ulaby, F. T., and M. A. EL-Rayes, "Microwave dielectric spectrum of vegetation, Part II: Dual dispersion model," *IEEE Trans. Geoscience and Remote Sensing*, GE-25, 550–57, 1987.
25. Newton, R. W., and J. W. Rouse, Jr., "Microwave radiometer measurements of soil moisture content," *IEEE Trans. Antennas and Propagation*, AP-28, 680-686, 1980.
26. Tsang, L., Z. Chen, S. Oh, R. Marks II, and A. Chang, "Inversion of snow parameters from passive microwave remote sensing measurements by a neural network trained with a multiple scattering model," *Proceedings of IGARSS'91*, 1965–1968, Espoo, Finland, 1991.
27. Tsang, L., "Polarimetric passive remote sensing of rough surfaces and discrete scatterers," *J. of Electromagnetic Waves and Applications*, Vol. 5, No. 1, 41–57, 1991.
28. Sarabandi, K., "Derivation of phase statistics of distributed targets from the averaged Mueller matrix," *Technical Report 026511-1-T*, Radiation Laboratory, Department of Electrical Engineering and Computer Science, University of Michigan, Ann Arbor, April 1991.

Leung Tsang received the SB (1971), SM, EE (1973), and Ph.D. (1976) from the Massachusetts Institute of Technology. He is presently a Professor of Electrical Engineering at the University of Washington. He is co-author of the book *Theory of Microwave Remote Sensing* Wiley-Interscience, 1985). He is on the editorial board of the *Journal of Electromagnetic Waves and Applications* (1987–1990), the *Journal of Waves in Random Media* (1990–present), an Associate Editor of *Radio Science* (1988–present) and an Associate Editor of the *IEEE Trans. on Geoscience and Remote Sensing* (1987–present). He is a Fellow of the IEEE and a member of the Electromagnetics Academy. His current research interests are in microwave remote sensing, waves in random media, and solid state theory of optoelectronics.

Chi Hou Chan attended Hong Kong Polytechnic and the City College of New York. He received the B.S. and M.S. degrees in electrical engineering from Ohio State University, Columbus, in 1981 and 1982, respectively, and the Ph.D. degree in electrical engineering from the University of Illinois at Urbana-Champaign, in 1987. He was a Visiting Assistant Professor associated with the Electromagnetic Communication Laboratory in the Department of Electrical and Computer Engineering at UIUC. Since September 1989, he has been an Assistant Professor of Electrical Engineering at the University of Washington, Seattle. He is a recipient of the Presidential Young Investigator award in 1991.

Jin Au Kong is Professor of Electrical Engineering and Chairman of Area IV on Energy and Electromagnetic Systems in the Department of Electrical Engineering and Computer Science at the Massachusetts Institute of Technology in Cambridge, Massachusetts. His research interest is in the field of electromagnetic wave theory and applications. He has published 7 books and over 300 refereed journal and conference papers, is the Editor of the Wiley Series in Remote Sensing, and is Chief Editor of the Elsevier book series

Progress In Electromagnetics Research (PIER).

James Joseph received his B.S. from the University of Kerala, M.S. from the University of Mississippi, and Ph.D. from the University of Illinois at Urbana-Champaign, all in Electrical Engineering. Since July 1990, he has been with the General Electric Corporate Research and Development Laboratory in Schenectady, New York. His current research interests include non-destructive testing of composite materials, electromagnetic and acoustic-scattering and radiation, and numerical methods.